Are control of extracellular acid-base balance and regulation of skeleton genes linked to resistance to ocean acidification in adult sea urchins?

Di Giglio S.[1], Spatafora D.[2], Milazzo M.[2], M'Zoudi S.[1], Zito. F.[3], Dubois Ph. [1]*, Costa C.* [3]

*these authors contributed equally

1. Laboratoire de Biologie Marine, Université Libre de Bruxelles, 1050 Bruxelles, Belgium.

2. Department of Earth and Marine Science (DiSTeM), Università degli studi di Palermo, 90146 Palermo, Italy

3. Consiglio Nazionale Delle Ricerche, Istituto per la Ricerca e per l'Innovazione Biomedica (IRIB), Via Ugo La Malfa 153, 90146, Palermo, Italy

Corresponding authors:

digiglio.sarah@gmail.com - 003226502517

phdubois@ulb.ac.be - 003226502970

caterina.costa@irib.cnr.it - 00390916574578

Paper type: Primary research

Keywords: Ocean acidification, CO_2 vent, Echinoderms, gene expression, qPCR, skeleton, mechanical properties, DIC

22 1. Introduction

23 Levels of carbon dioxide (CO_2) in the Earth atmosphere are increasing, mainly due to human
24 activities, and are expected to reach 485 to 900 ppm in 2100 (Jewett and Romanou, 2017;
25 Meinshausen et al., 2011). One-third of the CO_2 released in the atmosphere is absorbed by the
26 ocean and induces complex changes in the seawater chemistry, principally decreasing the
27 surface seawater pH and carbonate ion concentration, a phenomenon known as ocean
28 acidification (OA) (Orr et al., 2005). According to the IPCC RCP8.5 (Intergovernmental Panel
29 on Climate Change Representative Concentration Pathway8.5) - business-as-usual - scenario,
30 by the end of this century, a decrease up to 0.3 to 0.4 units of pH is expected, leading to a
31 surface seawater total scale pH (pH_T) 7.7. Direct and indirect effects of short and long-term
32 expositions to low pH differ according to the considered taxa, making overall predictions
33 difficult (Wittmann and Pörtner 2013). Calcifying metazoa with a low metabolism (therefore
34 with a poor machinery to eliminate CO_2 and protons) and osmoconformers (organisms whose
35 composition of extracellular fluids is close to that of seawater) were hypothesized to be
36 particularly vulnerable to OA (Pörtner 2008; Melzner et al. 2009; Kroeker et al. 2013).

37 Echinoderms cumulate these characteristics, including an extensive high-magnesium calcite
38 skeleton, and were therefore expected to be particularly affected by OA. Surprisingly, adult sea
39 urchins resist OA rather well, even at long-term (Kurihara et al. 2013; Dupont and Thorndyke
40 2013; Hazan et al. 2014; Moulin et al. 2015; Morley et al. 2016, Uthicke et al 2016, Manriquez
41 et al 2017). This is also true for the skeleton which, except for spines, appears protected from
42 OA (Dery et al. 2017 and references therein). This has been attributed to the ability of most sea
43 urchins to compensate their extracellular pH (pH_e), principally by accumulation of bicarbonate
44 ions, when facing OA (Stumpp et al. 2012; Collard et al 2013, 2014, 2016; Moulin et al. 2015;
45 Morley et al. 2016). Indeed, the ability to control the extracellular acid-base balance is
46 considered to be a key process in metazoans to tolerate OA (Pörtner 2008). It is worth

47 emphasizing that the echinoderm skeleton is an endoskeleton, embedded in the dermis and
48 covered by the epidermis, which confers some protection from OA (see Dery et al. 2017 for a
49 discussion). Furthermore, the expression of biomineralization-related genes in regenerating
50 spines of adult sea urchins was reported to be up-regulated when sea urchins were exposed to
51 very low pH_T (7.47), whereas there was no significant difference with control at pH_T 7.70
52 (Emerson et al. 2017).

53 However, not all sea urchins do control their acid-base balance when facing OA. In particular,
54 cidaroids, a basal clade of echinoids, and some basal euechinoids (the sister clade of cidaroids,
55 including most living sea urchins) do not compensate their pH_e and, actually, maintain a
56 particularly low pH_e whatever the seawater pH (Calosi et al. 2013; Collard et al. 2013, 2014).
57 Surprisingly, these species succeed very well in undersaturated environments (deep sea) or near
58 CO_2 vents. In particular, the basal euechinoid *Arbacia lixula* (Linnaeus 1758), which keeps a
59 low pH_e in acidified conditions, at least in 4-days experiments, maintains higher population
60 densities close to CO_2 vents than the sympatric sea urchin *Paracentrotus lividus* (Lamarck
61 1816), which is able to compensate its pH_e (Calosi et al. 2013, Bray et al. 2014). This couple
62 of sympatric species, occurring close to well-characterized CO_2 vents in the Mediterranean Sea,
63 offers an excellent opportunity to test to which extent the control of the acid-base balance
64 confers a protection towards OA and up to which point it affects the expression of
65 biomineralization-related genes and the mechanical function of the skeleton. Therefore, the
66 present study investigated the long-term acid-base physiology of individuals of both species
67 living in or out the plume of a cold volcanic CO_2 seep (Levante Bay, Vulcano Island, Sicily),
68 together with the impact on the mechanical properties of their skeleton and the expression of
69 biomineralization-related genes. Based on a number of Omic and functional genomic studies
70 performed on several sea urchin species (Consortium, 2006; Hogan et al., 2019; Karakostis et
71 al., 2016a; Livingston et al., 2006; Mann et al., 2008; Oliveri et al., 2008), four target genes

72 (*p19*, *msp130 sm50,* and *can*) with known roles in the biomineralization process of both
73 embryos and adults, and a housekeeping gene (*z12*), were selected for investigate the expression
74 profiles in the samples above described. Orthologous genes of *P. lividus* and *A. lixula*, known
75 or, here, preliminary identified and validated, provided the molecular tools of both species for
76 setting-up species-specific Real-Time qPCR assays performing the analyses of gene expression
77 here reported (for sequences identification and experimental setting see S01). The target genes
78 chosen code for well-known proteins involved in the skeletogenesis of sea urchin embryos and
79 larvae, namely an acidic protein (P19), a calcium ion transporter glycoprotein (the
80 mesenchyme-specific cell surface glycoprotein MSP130), a carbohydrate-binding C-type lectin
81 (spicule matrix protein SM50) and a carbonic anhydrase (CAN), involved in the conversion of
82 CO_2 to bicarbonate HCO_3^- ions (Costa et al., 2012; Karakostis et al., 2016a; Killian and Wilt,
83 2008; Livingston et al., 2006; V. Matranga et al., 2011). Expression of similar genes and
84 proteins has been reported during the formation of larval skeleton of the sea urchins
85 *Strongylocentrotus purpuratus* (Stimpson 1857) and *P. lividus* (Lamarck 1816), suggesting a
86 similar role in later life stages (Karakostis et al., 2016b; Livingston et al., 2006; Mann et al.,
87 2008).

88 This work is a contribution to understand the OA impacts on calcifying marine organisms. For
89 the first time, a combination of cutting-edge approaches highlighted intraspecific correlated
90 properties of acid-base regulation capacity of the coelomic fluid, calcitic skeleton integrity, and
91 gene expression in specimens of *P. lividus* and *A. lixula* from a naturally acidified site and a
92 control site. The results prompt towards new hypotheses on the effects of the impact of OA in
93 sea urchins.

94

2. Materials and Methods

2.1. Sampling and physico-chemical measurements

Adults sea urchins *P. lividus* and *A. lixula*, were collected in September 2018 by snorkelling between three and five meters depth in two sites (10 urchins per species per site) in the Levante Bay off Vulcano Island in the Mediterranean Sea (38°25'19'' N/14°57'59'' E) (Italy) (Fig.1), alongside with three seawater samples per site. One site is characterized by stable environmental conditions (Control) and the other is in an acidified area characterized by the presence of natural CO_2 vents (corresponding, respectively, to sites R1 and 20 fully described in Boatta et al. 2013). This site has already been used as a natural OA experiments laboratory in the past few years (*i.e.* Calosi, et al. 2013; Duquette et al. 2017; Milazzo et al. 2019). Our sampled adult organisms *P. lividus* and *A. lixula* (size of individuals from each species and site are presented in Table 2.) were taken at the pCO_2 intermediate levels (pH 7.6) because, as reported in Calosi et al. (2013), the density of both species in that area was appropriate and not to decimate the populations and to enable comparisons with organisms from the control site. Salinity, temperature, total-scale pH (pH_T) and the total alkalinity (TA) of seawater from the site were directly measured after sampling and seawater samples were stored at 4°C for further measurements of dissolved inorganic carbon (DIC). All measures followed methods described by Collard et al. (2014).

Sampled animals were kept inside aerated buckets filled with seawater from the sampling sites at 24°C for a few hours until their processing in the laboratory of the INGV (Istituto Nazionale di Geofisica e Vulcanologia) of Vulcano Island. Diameter at ambitus and height of the test were measured for each specimen using a Vernier caliper. The extracellular fluid of the coelomic cavity (= coelomic fluid = CF) was collected through the peristomial membrane using a 5 ml syringe. A part (500µl) was used to measure the pH_T and TA. The remaining fluid was enclosed

120 in Eppendorf tubes without air bubble and deprived of the cells by centrifugation at room
121 temperature and was stored for further analyses. All physico-chemical parameters
122 measurements of the coelomic fluid (CF) were carried out according to Collard et al. (2014).
123 Aragonite and calcite saturation states (Ω) as well as pCO_2 and the concentrations of the
124 carbonate system components in the sea water and these parameters together with TA in the CF
125 were calculated from DIC, pH (total scale), salinity and temperature data (measured in the
126 laboratory and corrected with the field data) using the software CO_2SYS (Pierrot et al., 2006)
127 with the dissociation constants for carbonate from Mehrbach et al. (1973) refitted by Dickson
128 and Millero (1987), and for KSO_4 from Dickson (1990).

129 Then, half of the test (with the spines) was dried in an oven at 50 °C for 24 hours and stored for
130 further experiments. The other half was cleaned from internal organs and spines with clear
131 seawater and one entire ambulacra was dissected and stored by immersion in RNA later™
132 Stabilization solution (Thermo Fisher) in a volume ratio of 1:5 at 4°C, to be used within 1 month
133 for RNA extractions.

134 2.2.Ossicle sampling and preparation for mechanical tests

135 The oven-dried sea urchin half test (spines and plates) were cleaned from soft tissues by
136 incubations in NaOCl 2.5% for 90 min., then in NaOCl 5.25%, for 90 min. for the spines and
137 150 min. for the plates; after that, all the ossicles were rinsed with Supra-pure water (Sartorius),
138 then air-dried for at least 24 hours before use.

139 Five spines, five ambital interambulacral plates, i.e. the middle largest plates, and five apical
140 plates, i.e. the smallest and the uppermost plates, the most recently formed, were detached from
141 each of the ten sampled sea urchins of both species and sites. In total, 50 ossicles of each type
142 per species per sites were sampled and submitted to mechanical tests.

2.3. Mechanical test methods

All mechanical tests were carried out at room temperature. Different mechanical characteristics were measured or calculated for all considered ossicles: the force at which the ossicles breaks (F_{max}), the stress at rupture ($\sigma = F_{max}$/fracture surface of the ossicles) and the apparent Young's modulus (E), characterizing the material stiffness, was calculated according to the linear-elastic beam theory:

$$E = \frac{stress}{strain} = \frac{\sigma}{\varepsilon} = \frac{F/A}{\Delta L/L}\ (Pa)$$

Where: σ: stress (Pa), ε: strain (dimensionless) F: force (N), A: area (in transverse section) (m^2), ΔL: deflexion or displacement (m), L: effective length (m).

Mechanical tests differed according to the considered ossicles, in order to mimic the forces applied to these on nature.

Ambital plates were tested using a three-point bending test as represented in Fig 2. in Collard et al. (2016) at a speed of 0.2 mm/min for loading the load frame. The apparent Young's modulus (E) of ambital plates was calculated with the formula:

$$E = \frac{F_{max}\, L_e^3}{48\, \Delta L\, I_2}\ (\mathrm{Pa})$$

Where: F_{max}: force at fracture (N), ΔL: displacement (m), L_e: effective length (m) and I_2: second moment of inertia (m^4).

I_2 is a description of the geometric distribution of material around a neutral plane of bending and reflects the proportion of stereom in the plate fracture surface (vs. pores).

$$I_2 = \int y^2\, dA\ (m^4)$$

Where: y: the distance to the neutral plane of bending (m) and A: the area (m^2).

It was measured on micrographs of fractured surfaces of the plates obtained in a scanning electron microscope, using the macro MomentMacro in the software ImageJ (Schneider et al., 2012).

Flexural stress of the ossicle in a beam under three-point bending was calculated following:

$$\sigma = E \,.\, \varepsilon = \frac{F_{max}\, L_e^2}{48\, I_2} \text{ (Pa)}$$

Where σ: the bending stress at fracture (Pa), E, Young's modulus (Pa), ε, the strain (=ΔL/L, dimensionless), F_{max}: force at fracture (N), ΔL: displacement (m), L_e: effective length (m) and I_2: second moment of inertia (m^4).

Spines were tested using a two-point bending test as described in Dery et al. (2017), the device used for this test was represented in Fig. 3 in Moureaux et al. (2011). The apparent Young's modulus E was calculated with the formula:

$$E = \left(\frac{F_{max}}{\Delta L_e}\right) \times \int_0^L \frac{(x - L_e)}{I_2(x)}\, dx \text{ (Pa)}$$

$$\text{with } I_2 = ax + b \text{ (m}^4\text{)}$$

with F_{max}: force at fracture, ΔL the displacement, L_e the effective length, and x the spine section position. The distribution of the material around the neutral fibre was calculated by integrating the equation of the second moment of area (due to conical shape of spines, I_2 varies according to position in the spine).

Apical plates were tested using a simple compression method as described in Collard et al. (2016). To determine the Young's modulus for the apical plates, the force–displacement curves were transformed into stress–strain curves using the following equations:

$$E_1 = \frac{\sigma_{\max} - \sigma_{100thpoint}}{\varepsilon_{\max} - \varepsilon_{100thpoint}} \text{ (Pa)}$$

185 The E_1 is calculated as the slope between two points of the final linear part of the curve, in this
186 case the maximum force and the 100th point before that.

187 Where: σ: stress (Pa) calculated as F_{max} /A (A= area of the tuberculae of the plate) and ε: strain
188 (dimensionless) calculated as $\Delta L/L_e$ (L_e = the height of the plate) as in Asnaghi et al. (2019).

189 2.4.Nanoindentation

190 Five ambital plates and five spines on each of the five individuals used for the gene expression
191 analyses from each species and each site were sampled. Once cleaned, the ossicles were
192 embedded in epoxy resin (Struers ®, Gmbh), then ultra-polished using sandpapers of increasing
193 grain size (from 180 to 2400, FEPA Struers®) and cerium oxide (3 µm) until the calcium
194 carbonate of the skeleton was exposed to the surface and properly polished. The obtained
195 sections were perpendicular to the growth axis. Three to ten useful indents were obtained in the
196 cross section of each ossicle by a nanoindenter (TriboIndenter, Hysitron, Minneapolis, MN,
197 USA) with a charge of 3000 µN using a Berkovich tip (Presser et al. (2010). Elastic modulus
198 (Young's modulus; E) and hardness (H) values of the calcite were determined from the
199 unloading curve of the indentation test (Oliver and Pharr, 1992).

200 2.5.Gene expression

201 2.5.1. RNA Extractions

202 In order to select a tissue to use for gene expression analysis, body wall and podia (containing
203 skeletal elements) taken from *P. lividus* and *A. lixula* were preliminarily used in RNA
204 extractions performed using the GenElute™ Mammalian Total RNA Miniprep Kit, following
205 the manufacturer instructions with some changes. Briefly, after removing RNA later solution,
206 ambulacral plates or podia skeletal ring were plunged and washed by pipetman in the lysis
207 solution containing 2-Mercaptoethanol (0.1%), for 2 min. The resulting lysate was further
208 homogenized in a 2 ml Dounce (Sigma Aldrich). After centrifugation at 13.000 rpm for 2 min.,

209 the pellet containing coarser particles was removed and the supernatant was loaded on the
210 filtration column of the kit to remove the remaining debris. DNA contamination was removed
211 after the RNA elution step by DNase reaction using the on column DNase I Digestion Set
212 (Sigma Aldrich), following the manufacturer instructions. The highest yield was obtained using
213 body wall tissue of both species. Therefore, total RNA extractions from the sampled sea urchins
214 of both species were performed using five ambulacral plates per specimen, following the
215 procedure described above. Two total RNA extractions were performed for each specimen.
216 Absence of contaminants (purity) and amount of total RNA extracted were estimated using the
217 D30 spectrophotometer (Eppendorf) at 260/280 nm and 260 nm, respectively. All samples were
218 frozen at −20 °C until use.
219

220 2.5.2.Synthesis of cDNA and preliminary amplifications (PCRs)

221 In preliminary real time qPCRs, cDNAs corresponding to 20ng, 15ng, 10ng and 5ng of total
222 RNA, were tested in addition to temperature, time and number of running cycles, in order to
223 ensure similar efficiency for target and reference genes. The primers shown in Table 1 and the
224 reference genes (*Pl-* and *Al-z12-1*) were also validated. Single pick ensuring the lack of primer-
225 dimers and primers specificity was shown in each melting curve; minimal threshold cycle (CT)
226 variability in both controls and acidified samples demonstrated that the reference genes were
227 unaffected by acidification conditions (Table S01.2.)

228 In a final reaction volume of 20 µl, cDNAs were derived from 500ng of total RNAs in a thermal
229 cycler using the High-Capacity cDNA Reverse Transcription Kits and random hexamer primers
230 (Applied Biosystems, Life technologies) according to the manufacturer's instructions. In total,
231 four cDNA preparations were performed for each specimen, two for each total RNA sample.
232 The synthesized cDNAs were frozen at −20 °C. Before using them in the gene expression
233 assays, aliquots were checked by amplification in preliminary Polymerase Chain Reaction

234 (PCR) with Red Taq Polymerase (Sigma Aldrich) following the manufacturer's instructions.
235 The NCBI GenBank Accession Numbers of the amplicons sequenced are reported in Table
236 S01.1.

237 2.5.3. Real Time qPCR Comparative Assays

238 The $2^{-\Delta\Delta Ct}$ method (Livak and Schmittgen, 2001) and SYBR Green chemistry were used in Real
239 time qPCRs comparative assays to measure the expression of the *P. lividus* and *A. lixula*
240 selected genes: *p19*, *msp130 sm50*, *can.* Step One Plus real time PCR Cycler Instrument
241 (Applied Biosystems) and the PFAST- R SY Precision FAST qPCR Master Mix with ROX and
242 SYBR green (Primerdesign Ltd) were used according to the manufacturer instructions. In
243 preliminary real time qPCRs, cDNAs corresponding to 20ng, 15ng, 10ng and 5ng of total RNA,
244 were tested in addition to temperature, time and number of running cycles, in order to ensure
245 similar efficiency for target and reference genes. The primers shown in Table 1 and the
246 reference genes (*Pl*- and *Al-z12-1*) were also validated. Single pick ensuring the lack of primer-
247 dimers and primers specificity was shown in each melting curve; minimal threshold cycle (CT)
248 variability in both controls and acidified samples demonstrated that the reference genes were
249 unaffected by acidification conditions (Table S01.2.).
250 In each real time qPCR comparative assay, the reactions were performed in a 96 wells plate, in
251 final volumes of 20 µl containing the same quantity of cDNA correspondent to 11.11 ng of total
252 RNA. Five independent biological replicates of both biological group (Control and Acidified)
253 of each species were run in the same plate. *Pl*- and *Al- z12-1* mRNAs (NCBI GenBank A.
254 Numbers LT900344.1 and MN917142), were used as reference genes, respectively, as well as
255 specimens from control site were used as calibrators (*Pl*-C and *Al*-C, respectively). Both, master
256 mix for each oligo couple and technical duplicates of each cDNA were used to test the
257 reproducibility of the qPCR technology. After optical adhesive film sealing (Applied
258 Biosystems, Life Technologies), the plate was briefly centrifuged (1.000 rpm for 2 min at

259 ambient temperature). The assay running was set as follows: 1×cycle: enzyme activation (hot
260 start), 2 min. at 95°C; 45×cycles: denaturation at 95 °C for 5 sec. plus annealing/extension at
261 60 °C for 20 sec., followed by a melting curve stage. For each cDNA preparation, two to five
262 qPCR assays were performed.
263 The data were collected and analyzed by StepOne Software v2.3 (Applied Biosystems). After
264 omitting the non-assessable wells according to the StepOne software setting, the final plate
265 layout was elaborated using as calibrator each of the five control specimens (*Pl*-C or *Al*-C) for
266 all acidified specimen (*Pl*-A or *Al*-A). The total number of comparisons within the same qPCR
267 assay was increased by using all the five control specimens one by one as calibrators (n
268 crossing). For each species, data from all qPCR assays were checked and the outlier's values
269 were omitted. The mean and standard deviation were calculated from all data obtained from the
270 assays from one acidified biological replicate for each gene. In the graphic representations
271 (Figures 3 and 4), the relative expression values of each gene are shown as the mean of all
272 acidified specimens.
273
274 2.6. Statistical analyses
275 All ANOVA models were built according to the recommendations of Doncaster and Davey
276 (2007) and followed by Tukey test using the appropriate mean square error for multiple
277 comparisons when ANOVA p-value was lower than 0.050. All tests were carried out using the
278 software Systat12 (Systat Software Inc., USA).
279 Physico-chemical parameters of the seawater sample were analysed with non-parametric
280 Kruskal-Wallis test. All data of physico-chemical and biometric parameters of the coelomic
281 fluid were submitted to two-factors ANOVA (species: crossed fixed factor, site: crossed fixed
282 factor). Relative gene expression was analysed using model III ANOVA (gene: fixed factor,
283 individual: random factor, crossed individual: random factor).

2.7. Weibull analysis

Because of the broad dispersion of results, material science usually uses the cumulative probability function to interpret mechanical results:

$$P_{f\,i} = 1 - \exp\left(-\left(\frac{\sigma_i}{\sigma_0}\right)^m\right)$$

Which is known as the Weibull three parameters strength distribution. P_f is the probability of failure that increases with the stress variable, σ. Weibull modulus, m, corresponds to the distribution of flaws within the specimen. The characteristic stress σ_0 is an experimentally obtained parameter that corresponds to a proportion of fractured samples of (1 – 1/e) = 63% (cumulative failure probability). In this study, this formula to stress (σ), force at fracture (F_{max}), Young's modulus (E), nanohardness (H) and nanoelasticity (E) was applied and the linearized curve of Weibull statistical analysis was used to calculate the 95% confidence intervals of the 63 percentile of each of the aforesaid variables, with the modified least square regression method of Bütikofer et al. (2015). This allowed statistical comparisons, based on the 95% confidence intervals, for each ossicle of each species and site.

3. Results

3.1. Carbonate chemistry of seawater and acid-base physiology of the sea urchin

Carbonate chemistry of seawater in Levante Bay on the day of sampling is reported in Table 2. Temperature ranged from 24.1 to 25.0°C and salinity was 37.2.

Seawater pH_T, carbonate concentration and saturation states of calcite and aragonite were significantly lower (p-value ≤ 0.046, S02), while concentrations of DIC and bicarbonate as well as partial pressure of CO_2 (pCO_2) were significantly higher at the acidified site (p-value ≤ 0.049). Seawater TA and carbon isotopic signature of DIC did not significantly differ between the two sites (p-value ≥ 0.827). The results are similar to those reported for the same sites during a long-term monitoring by Boatta et al. (2013).

The coelomic fluid from adults of the two species significantly differed in all acid-base variables, *P. lividus* showing the more basic values and *A. lixula* the more acidic ones ($p_{ANOVA} \leq 0.009$, Table 3, S03). In contrast, neither the site nor the interaction term between the site and the species had any significant effect on these variables ($p_{ANOVA} \geq 0.106$). Only the $\delta^{13}C$ of the coelomic fluid of both species was significantly more negative in the acidified site ($p_{ANOVA} = 0.027$, Table 3, S03). The isotopic signature of ^{13}C of seawater was significantly higher (positive) than that of the coelomic fluid of *P. lividus* and *A. lixula* in all sites ($p_{Tukey} < 10^{-3}$). The diameter and height of the test of the two species significantly differed ($p_{ANOVA} < 10^{-3}$) and the interaction term was significant for the diameter ($p_{ANOVA} = 0.018$, Table 3). *A. lixula* was always the smaller species ($p_{Tukey} \leq 0.034$).

3.2. Mechanical properties

The mechanical data was analysed using Weibull analysis, based on the cumulative probability function (see Materials and Methods) (Tables 4,5,6). Arithmetical means and standard deviations are presented in supporting materials (S04).

The Weibull modulus for stress, a measure of flaw distribution in the material, in ambital plates ranged between 1.362 and 1.896. Based on the 95% confidence interval (CI 95), the Weibull moduli were not significantly different between species nor sites. In contrast, the characteristic stress at rupture (σ_0) and the characteristic Young's modulus (E_0), a measure of the elasticity of the material, of ambital plates differed significantly between *A. lixula* from control and acidified sites, being higher at the control site (Table 4, S05). The force needed to break 63% of the ambital plates (F_{max0}) of *A. lixula* was higher at the control than at the acidified site but when corrected with the length (F_{max}/L_{e0}), the difference was not significant anymore (Table 5, S05). CI 95 of σ_0, E_0 and F_{max0} for ambital plates *of P. lividus* of the two sites overlapped (S05).

332 Based on the respective CI 95, the force needed to break 63% of the apical plates (F_{max0}) was
333 significantly higher for plates of *A. lixula* than for those of *P. lividus* from the same site but did
334 not differ according to sites (Table 5, S06). However, when corrected by the effective length
335 (L_e), F_{max}/L_{e0} did not differ significantly between species (S06). The characteristic Young's
336 modulus (E_0) of apical plates was not significantly different between species and sites (Table
337 5, S06).

338 For spines, based on their respective CI 95, the force needed to break 63% of the spines ($F_{max0,}$
339 and F_{max}/L_{e0}) and the characteristic Young's modulus (E_0) were significantly lower in spines of
340 *A. lixula* from acidified site than from control site (Table 5, S07). Confidence intervals of spine
341 mechanical properties of *P. lividus* from the two sites overlapped.

3.3.Nanoindentation

Characteristic nanoelasticity (E_0) and nanohardness (H_0) of the ambital plates were not significantly different between species nor sites based on their respective CI 95 (Table 6, Fig. 2A-B, S08, S09).

Characteristic nanoelasticity of the spines (E_0) was significantly higher in *P. lividus* at both sites than in *A. lixula* based on their respective CI 95 (Table 6, Fig. 2C-D, S08, S09) but site had no significant impact.

3.4.Gene expression analysis, Real Time qPCR comparative assays

In the preliminary expression analysis (One Step RT-PCR) of *p19, msp130, sm50, can* and *z12-1* genes, we used podia skeletal ring and tests of both species. The sequences of the validated products amplified from tests of *P. lividus* and *A. lixula* are presented in S01 with their NCBI GenBank Accession Numbers. Although we found all targeted genes expressed in both tissues, for the following expression analyses we only used the tests of the animals for practical facilities and to link the results to the mechanical data. In preliminary qPCRs, we validated *z12-1* genes of both species to be used as reference genes, as acidification did not affect their expression (S01 and Table S01.2.). Through the expression assays properly set, we found a high number of relative expression values for each acidified specimen. Figure 3 shows the results of the Real Time qPCR comparative assays from *P. lividus.* The expression levels of *p19* and *msp130* genes from the acidified site seem to increase with respect to the control site (calibrator), although the differences are not significant. Expression of *can* did not differ according to the site. On the contrary, the *sm50* gene showed a significant decreased expression level ($p_{ANOVA} < 10^{-3}$) with respect to the control site (calibrator). We found a different trend of expression in the *A. lixula* genes. In the Figure 4, the expression of all genes significantly decreased with respect to the specific calibrators ($p_{Tukey} \leq 0.005$, Fig. 4, S10, S11). In particular, *sm50* showed the lowest expression value of 0.317±0.120 (S10, S11).

4. Discussion

4.1. Acid-base physiology

A clear-cut difference in acid-base physiologies of the two species was evidenced for the first time for adult individuals living in acidified or control conditions, probably from their metamorphosis. Previous experiments reported results obtained after a few days exposure in acidified conditions for *A. lixula* (Calosi et al. 2013) or a few weeks for *P. lividus* (Catarino et al. 2012; Collard et al. 2013, 2014). *P. lividus* has a higher pH_e and lower pCO_2 than *A. lixula*, due to a much higher bicarbonate concentration in the coelomic fluid. These differences are not due to the respective sizes of individuals of both species. Indeed, *A. lixula* had a size similar to that of *P. lividus* in the control site and was significantly smaller in the acidification site. This means that *A. lixula* had a higher surface/volume ratio, which should allow a more efficient elimination of respiratory CO_2. Respiratory rates between the two species do not differ (Di Giglio, unpublished data). Therefore, higher pCO_2 in *A. lixula* CF is not due to this factor.

No differences in acid-base physiology of both species were evidenced between the control and acidified sites. On the one hand, it has been attributed to the bicarbonate buffering capacity of the CF in *P. lividus*, which is able to accumulate bicarbonate from seawater (Collard et al. 2014). On the other hand, *A. lixula* has a naturally close to 7.0 pH_e and pCO_2 around 4000-5000 µatm. As a consequence, the increased pCO_2 at the acidified site does not induce a significant reduction of the gradient allowing the diffusion of respiratory CO_2 out of the body, therefore avoiding or reducing an increase in CF pCO_2 (see Seibel and Walsh 2003). It is also noteworthy that CF alkalinity of *A. lixula* did not differ significantly between individuals of both sites and remained close to bicarbonate concentration, indicating that a non-bicarbonate buffer is not involved, contrary to the hypothesis of Calosi et al. (2013). Finally, the saturation states for calcite and aragonite are, respectively, equal and lower than 1 in the CF of *A. lixula* from the acidified site. Such condition is also observed in cidaroid sea urchins (Collard et al. 2014).

The difference in CF $\delta^{13}C$ between individuals of both species is intriguing because this variable did not differ according to site in seawater. Courtney and Ries (2015) showed a positive relation between $\delta^{13}C$ in the spine skeleton and pCO_2 in seawater. Here we had the opposite relation. This might match the dissolution hypothesis proposed by Courtney and Ries (2015), dissolved $CaCO_3$ molecules containing isotopically lighter ^{12}C-isotopes. This is making sense for *A. lixula* whose CF saturation states are low, but not for *P. lividus* whose CF Ω are larger or equal to 2. Another hypothesis is that food in both species differed according to sites. This could result from differences in $\delta^{13}C$ in food but the link is much more indirect than in usual stable isotopes studies (France, 1995; Ng et al., 2007). Indeed, our measures of $\delta^{13}C$ only concern CF DIC.

4.2.Impact on the skeleton

The mechanical properties of different parts of the skeleton of *P. lividus* did not differ between individuals from control and acidified sites. Regarding ambital and apical plates, this is in line with results of Collard et al. (2016) and Asnaghi et al. (2019). For spines, previous studies reported no mechanical effect at seawater pH_T higher than 7.5 despite corrosion evidence on the skeleton (Byrne and Fitzer, 2019; Dery et al., 2017; Emerson et al., 2017; Holtmann et al., 2013). On the contrary, ambital plates and spines of *A. lixula* from the acidified site showed reduced F_{max0} and E_0, meaning that those skeletal parts are less stiff and break more easily when formed in acidified conditions. However, effects on F_{max} disappeared when normalized by the effective length of the plates, indicating that the size of the skeletal elements were the drivers of the effects on F_{max}. Furthermore, ambital plates also showed a characteristic stress at rupture reduced by 42%, meaning that for normalized areas they are much more breakable. Surprisingly, the apical plates, the most recently formed test plates, did not show significant differences in their mechanical properties between individuals from control and acidified site. This could be due to the lower discriminant power of compression tests, compared to three-

point bending tests. Therefore, the functional properties of *A. lixula* skeleton (elasticity and stress at rupture) were impacted in acidified conditions and this occurred at a much higher seawater pH_T than previous effects reported in euehinoid species.

4.3. Impact on gene expression

Relative patterns of biomineralization-related genes expression in the sea urchin test strongly differed between the two species. Expression of these genes was not different in *P. lividus* from both sites except for *sm50*, which was downregulated, while all studied genes were downregulated in *A. lixula* from the acidified site. In adult, downregulation of several biomineralization-related genes appeared correlated to the recorded mechanical effects, strongly suggesting a cause-relationship effect.

These results contrast with those obtained by Emerson et al. (2017), who showed significant upregulations of biomineralization-related genes in regenerating spines of *L. variegatus*. However, this effect was only recorded at low seawater pH_T 7.47 and in actively regenerating spines, which are quite different conditions from those of the present study. Data on the expression of biomineralization-related genes in adult submitted to OA conditions is still poor, whereas the regulation of genes involved in embryos and larvae are more studied. Especially, researches focusing on the impact of OA on the expression of development-related genes increased recently, and highlighted a significant down-regulation of all kind of genes including biomineralization-related genes (Evans and Watson-Wynn 2014). Especially, Martin et al. (2011) showed a down-regulation of the *sm50* gene in embryos and larvae of *P. lividus* under OA, which has also been measured in adult *P. lividus* in the present study. Since the role of the protein SM50 has been defined to be the same in all *S. purpuratus* life stages (Killian and Wilt, 2008), further transgenerational studies could confirm the negative effect of OA on biomineralization-related genes from the larval to the adult stages.

4.4.Ecological impacts

A. lixula, which has a low pH_e with low buffering capacity, were more affected from OA than *P. lividus*, which is endowed with a much higher buffering capacity in its extracellular fluids. By contrast, *A. lixula* maintained higher population density in acidified sites than *P. lividus* (Calosi et al. 2013, personnal observations). Sympatric sea urchins of Mediterranean Sea, *A. lixula* and *P. lividus* coexist on the rocky shore because of the low overlap of their diet, respectively herbivorous and omnivorous, leading to a niche differentiation (Agnetta et al., 2013; Benedetti-Cecchi and Cinelli, 1995; Bulleri et al., 1999; Palacín et al., 1998). Their food web role are different but their density of population are similar in most natural environments, except near CO_2 vents where *P. lividus* is less present than *A. lixula* (Calosi et al. 2013; Bray et al. 2014). Calosi et al. (2013) rejected the hypotheses based on food availability, predation or human harvesting. García et al. (2015) highlighted a difference in the settlement of larval *P. lividus* and *A. lixula* due to the effect of low pH. They observed that *P. lividus* settlement was delayed because of the stress and hypercapnic conditions that alter the composition of settlement inducers, such as crustose coralline algae or bacterial biofilms (Webster et al., 2013), but the same stressors had no consequences for the settlement of *A. lixula*. However, Privitera et al. (2011) did not highlight any difference on the metamorphosis (from larvae to juvenile) rate of *P. lividus* according to the substrate, whereas *A. lixula* showed a different rate when settling on naked stones or encrusting coralline algae. These hypotheses might explain why *P. lividus* population is less dense at high pCO_2 site, although none of the characteristics studied in this work were impaired by OA, except for the down expression of the biomineralization-gene *sm50*. This could be linked with a different strategy of survival than *A. lixula* population, in which the four studied biomineralization-related genes were significantly downregulated and the skeletal spine properties were significantly affected. Indeed, higher densities of *A. lixula* in the acidified sites might be linked to a better settlement of larvae in acidified conditions

(Wangensteen et al., 2012). However, this does not mean that performances are similar in control and acidified sites. In particular, significantly smaller sizes of *A. lixula* in the acidified site may be due to either reduced growth or increased predation of larger size classes linked to reduced mechanical strength, smaller individuals escaping this by hiding in cracks and holes. Resource allocation to reproduction in acidified sites should also be questioned (García et al., 2018; George, 1990; Visconti et al., 2017). Finally, these higher densities of *A. lixula* at acidified sites might be only possible thanks to reservoirs of successfully reproducers outside the acidified zone.

5. Conclusion

In the two species studied here, it appeared that *P. lividus*, which has a high bicarbonate buffering capacity in its extracellular fluids, is much less affected than *A. lixula* which has a weak buffering capacity. Actually, adult *A. lixula* showed effects at much higher seawater pH_T values than any other adult sea urchin species studied so far. Therefore, the capacity to regulate the acid-base physiology has major role in resistance to OA. However, the distributions of both species around the vent at Vulcano point to the importance to consider all the ecological aspects as the recruitment ecology to avoid misleading conclusions concerning the adaptation of populations to an acidified habitat.

6. Conflict of interest

All the authors of this paper declare that they have no conflicts of interest.

7. Acknowledgments

SD. is a holder of a FRIA grant. Ph. Dubois is a Research Director of the National Fund for Scientific Research (FRS-FNRS; Belgium). We would like to thank Professors I. Eeckhaut and P. Flammang and N. Puozzo for providing access to the SEM, S. De Kegel for her help with the preparation of resins for nanoindentation experiments; Dr.. S. Godet for the access the

nanoindentation devices, F. Dehairs and Dr. D. Verstraeten for the access to the IRMS for DIC and $\delta^{13}C$ measurements and M. Biondo and M. Bauwens for technical support. This study was supported by FNRS grant No. J.0219.16 SOFTECHI.

8. References

Agnetta, D., Bonaviri, C., Badalamenti, F., Scianna, C., Vizzini, S., Gianguzza, P., 2013. Functional traits of two co-occurring sea urchins across a barren/forest patch system. J. Sea Res. 76, 170–177. https://doi.org/10.1016/j.seares.2012.08.009

Asnaghi, V., Collard, M., Mangialajo, L., Gattuso, J.P., Dubois, P., 2019. Bottom-up effects on biomechanical properties of the skeletal plates of the sea urchin Paracentrotus lividus (Lamarck, 1816) in an acidified ocean scenario. Mar. Environ. Res. 144, 56–61. https://doi.org/10.1016/j.marenvres.2018.12.002

Benedetti-Cecchi, Cinelli, F., 1995. Habitat heterogeneity, sea urchin grazing and the distribution of algae in littoral rock pools on the west coast of Italy (Western Mediterranean). Mar. Ecol. Prog. Ser. 131, 219. https://doi.org/10.1016/S0140-6736(02)25581-6

Boatta, F, Alessandro, W.D., Gagliano, A.L., Liotta, M., Milazzo, M., Rodolfo-metalpa, R., Hall-spencer, J.M., Parello, F., 2013. Geochemical survey of Levante Bay , Vulcano Island (Italy), a natural laboratory for the study of ocean acidification. Mar. Pollut. Bull. 1–10. https://doi.org/10.1016/j.marpolbul.2013.01.029

Bray, L., Pancucci-Papadopulou, M.A., Hall-Spencer, J.M., 2014. Sea urchin response to rising pCO2 shows ocean acidification may fundamentally alter the chemistry of marine skeletons. Mediterr. Mar. Sci. 15, 510–519. https://doi.org/10.12681/mms.579

Bulleri, F., Benedetti-Cecchi, L., Cinelli, F., 1999. Grazing by the sea urchins Arbacia lixula L. and Paracentrotus lividus Lam. in the Northwest Mediterranean. J. Exp. Mar. Bio. Ecol. 241, 81–95. https://doi.org/10.1016/S0022-0981(99)00073-8

Bütikofer, L., Stawarczyk, B., Roos, M., 2015. Two regression methods for estimation of a two-parameter Weibull distribution for reliability of dental materials. Dent. Mater. 31, e33–e50. https://doi.org/10.1016/j.dental.2014.11.014

Byrne, M., Fitzer, S.C., 2019. The impact of environmental acidification on the microstructure and mechanical integrity of marine invertebrate skeletons. Conserv. Physiol. 7, coz062. https://doi.org/10.1093/conphys/coz062

Calosi, P, Rastrick, S.P.S., Graziano, M., Thomas, S.C., Baggini, C., Carter, H. a, Hall-Spencer, J.M., Milazzo, M., Spicer, J.I., 2013. Distribution of sea urchins living near shallow water CO2 vents is dependent upon species acid-base and ion-regulatory abilities. Mar. Pollut. Bull. 73, 470–484. https://doi.org/10.1016/j.marpolbul.2012.11.040

Catarino, A.I., Bauwens, M., Dubois, P., 2012. Acid-base balance and metabolic response of the sea urchin Paracentrotus lividus to different seawater pH and temperatures. Environ. Sci. Pollut. Res. Int. 19, 2344–53.

Collard, M., Dery, A., Dehairs, F., Dubois, P., 2014. Comparative Biochemistry and Physiology , Part A Euechinoidea and Cidaroidea respond differently to ocean acidi fi cation. Comp. Biochem. Physiol. Part A 174, 45–55. https://doi.org/10.1016/j.cbpa.2014.04.011

Collard, M., Laitat, K., Moulin, L., Catarino, A.I., Grosjean, P., Dubois, P., 2013. Buffer capacity of the coelomic fluid in echinoderms. Comp. Biochem. Physiol. - A Mol. Integr. Physiol. 166, 19–206. https://doi.org/10.1016/j.cbpa.2013.06.002

Collard, M., Rastrick, S.P.S., Calosi, P., Demolder, Y., Dille, J., Findlay, H.S., Hall-Spencer, J.M., Milazzo, M., Moulin, L., Widdicombe, S., Dehairs, F., Dubois, P., 2016. The impact of ocean acidification and warming on the skeletal mechanical properties of the sea urchin *Paracentrotus lividus* from laboratory and field observations. ICES J. Mar. Sci. J. du Cons. 73, 727–738. https://doi.org/10.1093/icesjms/fsv018

Consortium, S.U.G.S., 2006. The Genome of the Sea Urchin. Science (80-.). 314, 941–952. https://doi.org/10.1126/science.1133609

Costa, C., Karakostis, K., Zito, F., Matranga, V., 2012. Phylogenetic analysis and expression patterns of p16 and p19 in Paracentrotus lividus embryos. Dev. Genes Evol. 222, 245–251. https://doi.org/10.1007/s00427-012-0405-9

Courtney, T., Ries, J.B., 2015. Impact of atmospheric pCO2, seawater temperature, and calcification rate on the δ18O and δ13C composition of echinoid calcite (Echinometra viridis). Chem. Geol. 411, 228–239. https://doi.org/10.1016/j.chemgeo.2015.06.030

Dery, A., Collard, M., Dubois, P., 2017. Ocean Acidification Reduces Spine Mechanical Strength in Euechinoid but Not in Cidaroid Sea Urchins. Environ. Sci. Technol. 51, 3640–3648. https://doi.org/10.1021/acs.est.6b05138

Doncaster, C.P., Davey, A.J.H., 2007. Analysis of variance and covariance: how to choose and construct models for the life sciences. https://doi.org/10.1080/02664760902885203

Dupont, S.T., Thorndyke, M.C., 2013. Direct impacts of near-future ocean acidification on sea urchins. Clim. Chang. Perspect. from Atl. past, Present Futur. 461–485.

Duquette, A., McClintock, J.B., Amsler, C.D., Pérez-Huerta, A., Milazzo, M., Hall-Spencer, J.M., 2017. Effects of ocean acidification on the shells of four Mediterranean gastropod species near a CO2seep. Mar. Pollut. Bull. 124, 917–928.

https://doi.org/10.1016/j.marpolbul.2017.08.007

Emerson, C.E., Reinardy, H.C., Bates, N.R., Bodnar, A.G., 2017. Ocean acidification impacts spine integrity but not regenerative capacity of spines and tube feet in adult sea urchins. R. Soc. Open Sci. 4. https://doi.org/10.1098/rsos.170140

Evans, T.G., Chan, F., Menge, B.A., Hofmann, G.E., 2013. Transcriptomic responses to ocean acidification in larval sea urchins from a naturally variable pH environment. Mol. Ecol. 22, 1609–1625. https://doi.org/10.1111/mec.12188

Evans, T.G., Watson-Wynn, P., 2014. Effects of seawater acidification on gene expression: Resolving broader-scale trends in sea urchins. Biol. Bull. 226, 237–254. https://doi.org/10.1086/BBLv226n3p237

France, R.L., 1995. Carbon-13 enricment n benthic compared to planktonic algae: foodweb implications. Mar. Ecol. Prog. Ser. 124, 307–312. https://doi.org/10.3354/meps124307

García, E., Hernández, J.C., Clemente, S., 2018. Robustness of larval development of intertidal sea urchin species to simulated ocean warming and acidification. Mar. Environ. Res. in press. https://doi.org/10.1016/j.marenvres.2018.04.011

García, E., Hernández, J.C., Clemente, S., Cohen-Rengifo, M., Hernández, C.A., Dupont, S., 2015. Robustness of Paracentrotus lividus larval and post-larval development to pH levels projected for the turn of the century. Mar. Biol. 162, 2047–2055. https://doi.org/10.1007/s00227-015-2731-8

George, S.B., 1990. Population and seasonal differences in egg quality of arbacia lixula (Echinodermata: Echinoidea). Invertebr. Reprod. Dev. 17, 111–121. https://doi.org/10.1080/07924259.1990.9672098

Hazan, Y., Wangensteen, O.S., Fine, M., 2014. Tough as a rock-boring urchin: adult

Echinometra sp. EE from the Red Sea show high resistance to ocean acidification over long-term exposures. Mar. Biol. 161, 2531–2545. https://doi.org/10.1007/s00227-014-2525-4

Hogan, J.D., Keenan, J.L., Luo, L., Hawkins, D.Y., Ibn-, J., Lamba, A., Schatzberg, D., Piacentino, M.L., Zuch, D.T., Core, A.B., Blumberg, C., Timmermann, B., Grau, J.H., Speranza, E., Andrade-narravo, M.A., Irie, N., Poustka, A.J., 2019. The Developmental Transcriptome for Lytechinus variegatus Exhibits Temporally Punctuated Gene Expression Changes. bioRxiv.

Holtmann, W.C., Stumpp, M., Gutowska, M.A., Syré, S., Himmerkus, N., Melzner, F., Bleich, M., 2013. Maintenance of coelomic fluid pH in sea urchins exposed to elevated CO 2 : The role of body cavity epithelia and stereom dissolution. Mar. Biol. 160, 2631–2645. https://doi.org/10.1007/s00227-013-2257-x

Jewett, L., Romanou, A., 2017. Ocean Acidification and Other Ocean Changes. Clim. Sci. Spec. Rep. Fourth Natl. Clim. Assessment, Vol. I I, 364–392. https://doi.org/10.7930/J0QV3JQB

Karakostis, K., Costa, C., Zito, F., Brümmer, F., Matranga, V., 2016a. Characterization of an Alpha Type Carbonic Anhydrase from Paracentrotus lividus Sea Urchin Embryos. Mar. Biotechnol. 18, 384–395. https://doi.org/10.1007/s10126-016-9701-0

Karakostis, K., Zanella-Cléon, I., Immel, F., Guichard, N., Dru, P., Lepage, T., Plasseraud, L., Matranga, V., Marin, F., 2016b. A minimal molecular toolkit for mineral deposition? Biochemistry and proteomics of the test matrix of adult specimens of the sea urchin Paracentrotus lividus. J. Proteomics 136, 133–144. https://doi.org/10.1016/j.jprot.2016.01.001

Killian, C.E., Wilt, F.H., 2008. Molecular aspects of biomineralization of the echinoderm

endoskeleton. Prog. Mol. Subcell. Biol. 52, 199–223. https://doi.org/10.1007/978-3-642-21230-7_7

Kroeker, K.J., Kordas, R.L., Crim, R., Hendriks, I.E., Ramajo, L., Singh, G.S., Duarte, C.M., Gattuso, J.-P., 2013. Impacts of ocean acidification on marine organisms: quantifying sensitivities and interaction with warming. Glob. Chang. Biol. 19, 1884–1896. https://doi.org/10.1111/gcb.12179

Kurihara, H., Yin, R., Nishihara, G.N., Soyano, K., Ishimatsu, A., 2013. Effect of ocean acidification on growth, gonad development and physiology of the sea urchin Hemicentrotus pulcherrimus. Aquat. Biol. 18, 281–292. https://doi.org/10.3354/ab00510

Livak, K.J., Schmittgen, T.D., 2001. Analysis of relative gene expression data using real-time quantitative PCR and the 2-ΔΔCT method. Methods 25, 402–408. https://doi.org/10.1006/meth.2001.1262

Livingston, B.T., Killian, C.E., Wilt, F., Cameron, a, Landrum, M.J., Ermolaeva, O., Sapojnikov, V., Maglott, D.R., Buchanan, a M., Ettensohn, C. a, 2006. A genome-wide analysis of biomineralization-related proteins in the sea urchin Strongylocentrotus purpuratus. Dev. Biol. 300, 335–48. https://doi.org/10.1016/j.ydbio.2006.07.047

Mann, K., Poustka, A.J., Mann, M., 2008. The sea urchin (Strongylocentrotus purpuratus) test and spine proteomes. Proteome Sience 6, 22–32. https://doi.org/10.1186/1477-5956-6-22

Martin, S., Richier, S., Pedrotti, M.-L., Dupont, S., Castejon, C., Gerakis, Y., Kerros, M.-E., Oberhänsli, F., Teyssié, J.-L., Jeffree, R., Gattuso, J.-P., 2011. Early development and molecular plasticity in the Mediterranean sea urchin Paracentrotus lividus exposed to CO2-driven acidification. J. Exp. Biol. 214, 1357–68. https://doi.org/10.1242/jeb.051169

Matranga, V., Bonaventura, R., Costa, C., Karakostis, K., Pinsino, A., Russo, R., Zito, F.,

2011. Echinoderms as blueprints for biocalcification: regulation of skeletogenic genes and matrices. Prog. Mol. Subcell. Biol. 52, 225–248.

Meinshausen, M., Smith, S.J., Calvin, K., Daniel, J.S., Kainuma, M.L.T., Lamarque, J., Matsumoto, K., Montzka, S.A., Raper, S.C.B., Riahi, K., Thomson, A., Velders, G.J.M., van Vuuren, D.P.P., 2011. The RCP greenhouse gas concentrations and their extensions from 1765 to 2300. Clim. Change 109, 213–241. https://doi.org/10.1007/s10584-011-0156-z

Melzner, F., Gutowska, M.A., Langenbuch, M., Dupont, S., Lucassen, M., Thorndyke, M.C., Bleich, M., Pörtner, H.-O., 2009. Physiological basis for high CO2 tolerance in marine ectothermic animals: pre-adaptation through lifestyle and ontogeny? Biogeosciences Discuss. https://doi.org/10.5194/bgd-6-4693-2009

Milazzo, M., Alessi, C., Quattrocchi, F., Chemello, R., D'Agostaro, R., Gil, J., Vaccaro, A.M., Mirto, S., Gristina, M., Badalamenti, F., 2019. Biogenic habitat shifts under long-term ocean acidification show nonlinear community responses and unbalanced functions of associated invertebrates. Sci. Total Environ. 667, 41–48. https://doi.org/10.1016/j.scitotenv.2019.02.391

Morley, S.A., Suckling, C.C., Clark, M.S., Cross, E.L., Peck, L.S., 2016. Long-term effects of altered pH and temperature on the feeding energetics of the Antarctic sea urchin, Sterechinus neumayeri. Biodiversity 17, 34–45. https://doi.org/10.1080/14888386.2016.1174956

Moulin, L., Grosjean, P., Leblud, J., Batigny, A., Collard, M., Dubois, P., 2015. Long-term mesocosms study of the effects of ocean acidification on growth and physiology of the sea urchin Echinometra mathaei. Mar. Environ. Res. 103, 103–114. https://doi.org/10.1016/j.marenvres.2014.11.009

Moureaux, C., Simon, J., Mannaerts, G., Catarino, A.I., Pernet, P., Dubois, P., 2011. Effects of field contamination by metals (Cd, Cu, Pb, Zn) on biometry and mechanics of echinoderm ossicles. Aquat. Toxicol. 105, 698–707. https://doi.org/10.1016/j.aquatox.2011.09.007

Ng, J., Tak-Cheung, W., Gray, A.W., 2007. The effects of acidification on the stable isotope signatures of marine algae and molluscs. Mar. Chem. 103, 97–102. https://doi.org/10.1016/j.marchem.2006.09.001

O'Donnell, M., Todgham, A., Sewell, M., Hammond, L., Ruggiero, K., Fangue, N., Zippay, M., Hofmann, G., 2010. Ocean acidification alters skeletogenesis and gene expression in larval sea urchins. Mar. Ecol. Prog. Ser. 398, 157–171. https://doi.org/10.3354/meps08346

Oliver, G.M., Pharr, W.C., 1992. Measurement of Thin Film Mechanical Properties Using Nanoindentation. MRS Bull. 17, 28–33.

Oliveri, P., Tu, Q., Davidson, E.H., 2008. Global regulatory logic for specification of an embryonic cell lineage. Proc. Natl. Acad. Sci. U. S. A. 105, 5955–62. https://doi.org/10.1073/pnas.0711220105

Orr, J.C., Fabry, V.J., Aumont, O., Bopp, L., Doney, S.C., Feely, R.M., Gnanadesikan, A., Gruber, N., Ishida, A., Key, R.M., Lindsay, K., Maier-reimer, E., Matear, R., Monfray, P., Mouchet, a., Najjar, R.G., Plattner, G.K., Rodgers, K.B., Sabine, C.L., Sarmiento, J.L., Schlitzer, R., Slater, R.D., Totterdell, I.J., Weirig, M.F., Yamanaka, Y., Yool, a., Matear, Richard, 2005. Anthropogenic Decline in High-Latitude Ocean Carbonate by 2100. Nature 437, 681–686.

Palacín, C., Giribet, G., Carner, S., Dantart, L., Turon, X., 1998. Low densities of sea urchins influence the structure of algal assemblages in the western Mediterranean. J. Sea Res. 39,

281–290. https://doi.org/10.1016/S1385-1101(97)00061-0

Pierrot, D., Lewis, E., Wallace, D.W.R., 2006. MS Excel program developed for CO2 system calculations, in: ORNL/CDIAC-105a. Carbon Dioxide Information Analysis Center, Oak Ridge National Laboratory, US Department of Energy, Oak Ridge, Tennessee.

Pörtner, H, 2008. Ecosystem effects of ocean acidification in times of ocean warming: a physiologist's view. Mar. Ecol. Prog. Ser. 373, 203–217. https://doi.org/10.3354/meps07768

Presser, V., Gerlach, K., Vohrer, A., Nickel, K.G., Dreher, W.F., 2010. Determination of the elastic modulus of highly porous samples by nanoindentation: A case study on sea urchin spines. J. Mater. Sci. 45, 2408–2418. https://doi.org/10.1007/s10853-010-4208-y

Privitera, D., Noli, M., Falugi, C., Chiantore, M., 2011. Benthic assemblages and temperature effects on Paracentrotus lividus and Arbacia lixula larvae and settlement. J. Exp. Mar. Bio. Ecol. 407, 6–11. https://doi.org/10.1016/j.jembe.2011.06.030

Schneider, C.A., Rasband, W.S., Eliceiri, K., 2012. NIH Image to ImageJ: 25 years of image analysis. Nat. Methods 9(7), 671–675.

Seibel, B.A., Walsh, P.J., 2003. Biological impacts of deep-sea carbon dioxide injection inferred from indices of physiological performance. J. Exp. Biol. 206, 641–650. https://doi.org/10.1242/jeb.00141

Stumpp, M., Hu, M.Y., Melzner, F., Gutowska, M.A., Dorey, N., Himmerkus, N., Holtmann, W.C., Dupont, S.T., Thorndyke, M.C., Bleich, M., 2012. Acidified seawater impacts sea urchin larvae pH regulatory systems relevant for calcification. Proc. Natl. Acad. Sci. 109, 18192–18197. https://doi.org/10.1073/pnas.1209174109

Visconti, G., Gianguzza, F., Butera, E., Costa, V., Vizzini, S., Byrne, M., Gianguzza, P.,

2017. Morphological response of the larvae of Arbacia lixula to near-future ocean warming and acidification. ICES J. Mar. Sci. 8, 1–8. https://doi.org/10.1093/icesjms/fsx037

Wangensteen, O.S., Turon, X., Pérez-Portela, R., Palacín, C., 2012. Natural or Naturalized? Phylogeography Suggests That the Abundant Sea Urchin Arbacia lixula Is a Recent Colonizer of the Mediterranean. PLoS One 7, 1–16. https://doi.org/10.1371/journal.pone.0045067

Webster, N.S., Uthicke, S., Botté, E., Flores, F., Negri, A.P., 2013. Ocean acidification reduces induction of coral settlement by crustose coraline algae. Glob. Chang. Biol. 19, 303–315. https://doi.org/10.1111/gcb.12008

Wittmann, A.C., Pörtner, H.O., 2013. Sensitivities of extant animal taxa to ocean acidification. Nat. Clim. Chang. 3, 995–1001. https://doi.org/10.1038/nclimate1982

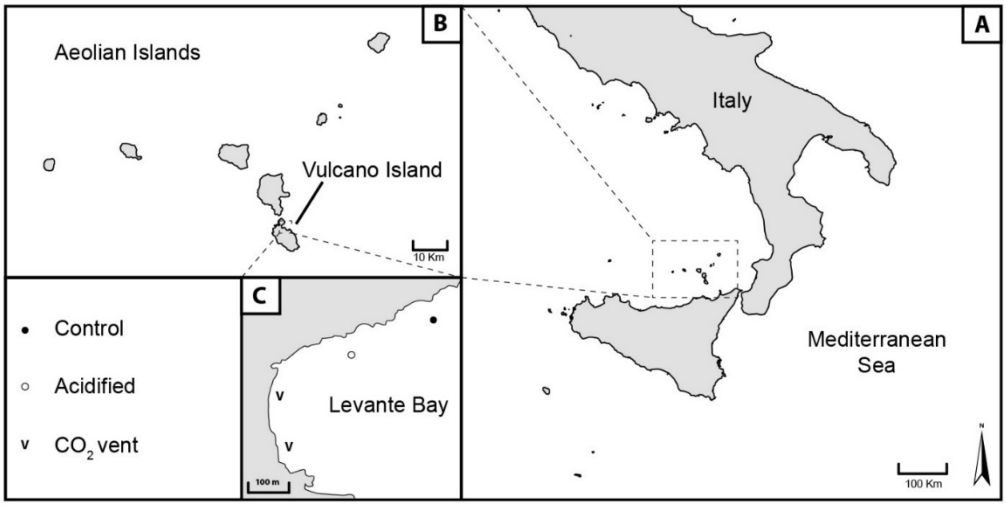

Figure 1. Sampling area **(A)** Global map of South Italy ; **(B)** Aeolian Islands; **(C)** Levante Bay (sampling sites marked with a dot).

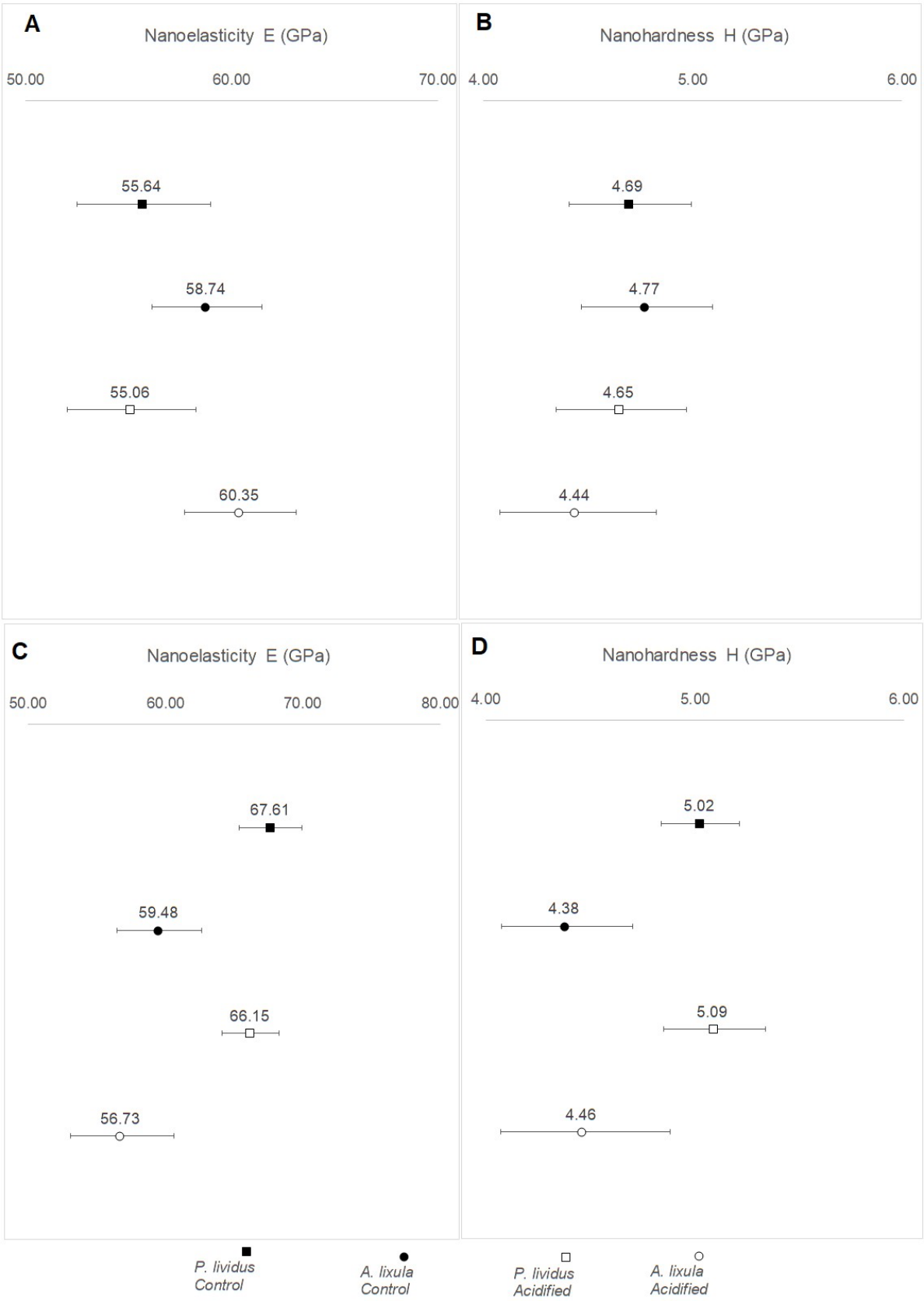

Figure 2. Characteristic nanoelasticity (E_0) and nanohardness (H_0) of the ambital plates (A,B) and of the spines (C, D) and their 95% confidence intervals for species and site according to Butikofer et al. 2015.

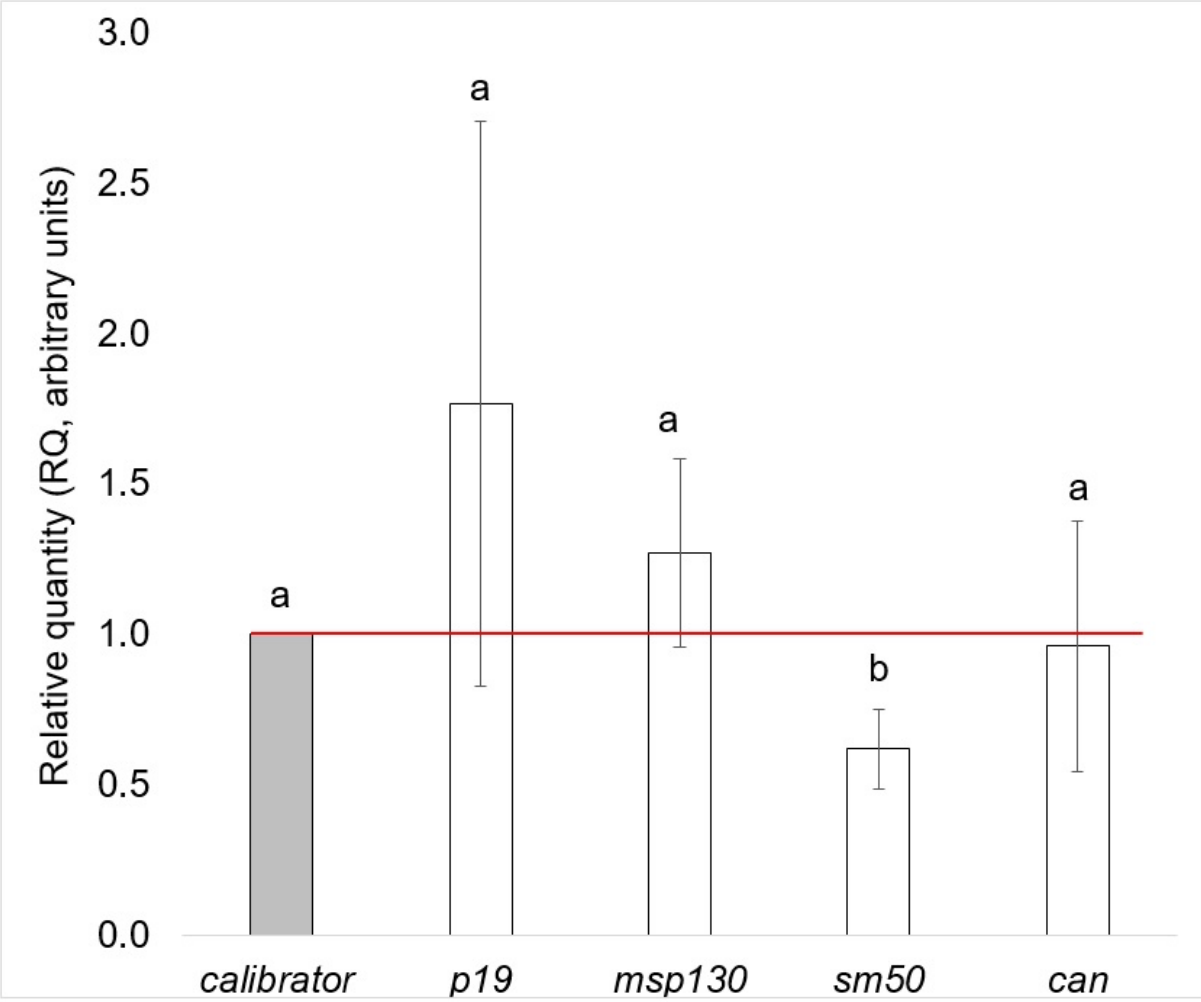

Figure 3. Relative Real Time qPCR assays on cDNA of *P.lividus* tests. Relative quantity (RQ) of *p19, msp130, sm50* and *can* gene expression. The graphic shows the means ± Standard deviation (SD) (n=5) of the results obtained from all performed assays for comparison of the genes expressed in specimens from acidified site with the same genes expressed in specimens from control site used as calibrator and set as 1 in arbitrary units. The *Pl-z12-1 mRNA* was used as an internal endogenous reference gene. Means sharing the same superscript do not differ significantly.

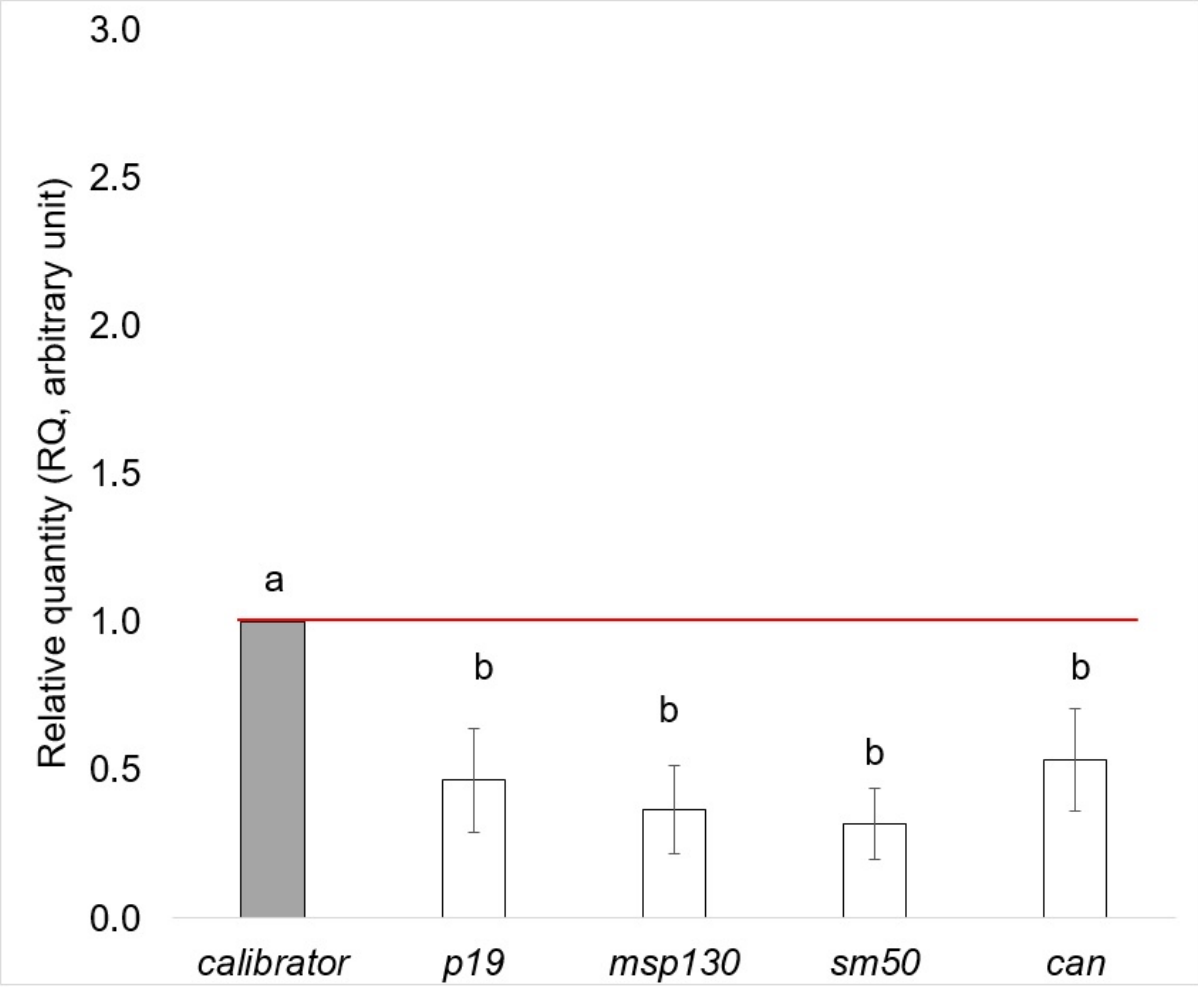

Figure 4. Relative Real Time qPCR assays on cDNA of *A.lixula* tests (mean ± sd, n=5). Relative quantity (RQ) of *p19, msp130, sm50* and *can* gene expression. The graphic shows the means of the results obtained from all performed assays for comparison of the genes expressed in specimens from acidified site with the same genes expressed in specimens from control site used as calibrator and set as 1 in arbitrary units. The A*l-z12-1 mRNA* was used as an internal endogenous reference gene. Means sharing the same superscript do not differ significantly.

Primers of biomineralization genes sequences utilized in One Step RT-PCR and Real Time qPCR assays

Gene name	Forward 5'-3'	Reverse 5'-3'	Amplicon
Pl-Z12-1	AGCGCCACACCAAAAGAAGTC	GGATGATAGACAGGGCTGTTTGGA	93
Pl- p19	GCAGGAGACTAAGACAGAGAC	CTCCGCTCGCCTCTCCTT	83
Pl-msp130	GTTGACCCCGTAACCATGAAC	GGGAAGAACTTTGCAACCTCC	80
Pl-sm50	CCGTGAACGCACAAAATCC	GGGCCTGACGCTTCATGA	64
Pl-can	CCAAAATGCTGGGAAAGTGTAAC	TCGGAACATGTCAAGCTGATTATG	81
Al -Z12-1	GTCTGCCTGAAGACCTTCGC	GAAAGACTTCCCGCATTCCTC	102
Al -p19	GAGAGCACGAGAGGGGAAC	GCGTCCATCTCAGCCTCC	102
Al -msp130	GGGTCCTGAGTGCGAGTC	GATGGCGAGAGCGCTGAC	91
Al -sm50	CCGTGAACGCACAAAATCC	GGGCCTGACGCTTCATGA	64
Al -can	CCAAAATGCTGGGAAAGTGTAAC	TCGGAACATGTCAAGCTGATTATG	81

Table 2. Seawater physico-chemical parameters at control and acidified sites on the day of sea urchins sampling (Mean ± SD, n=3) at Levante Bay

Site	Control	Acidified	p-value
pH_T (total scale)	7.93 ± 0.03	7.63 ± 0.05	**0.049**
TA (µmolkg-1)	2742 ± 167	2663 ± 29	0.827
DIC (mM)	2.37 ± 0.01	2.54 ± 0.06	**0.049**
pCO_2 (µatm)	594 ± 50	1327 ± 145	**0.049**
$[HCO_3^-]$ (mM)	2093 ± 15	2325 ± 49	**0.049**
$[CO_3^{2-}]$ (mM)	201 ± 14	115 ± 14	**0.049**
δ13C	1.08 ± 0.24	1.02 ± 0.03	0.827
Ω Calcite	4.75 ± 0.33	2.72 ± 0.32	**0.046**
Ω Aragonite	3.13 ± 0.22	2.32 ± 0.37	**0.049**

Table 3. Acid-base physiology of the coelomic fluid and biometry of adult sea urchins *P. lividus* and *A. lixula* at control and acidified sites (Mean ± SD) in Levante Bay. TA: total alkalinity (µmolkg^{-1}, n=3), DIC: concentration of dissolved inorganic carbon (mM, n=8), $[HCO_3^-]$: concentration of bicarbonate ions (mM, n=8), $[CO_3^{2-}]$: concentration of carbonate

ions (mM, n=8), $\delta^{13}C$: isotopic ratio of carbon 13 (‰, n=8), Ω Calcite : saturation state of calcite, Ω Aragonite : saturation state of aragonite. Means sharing the same superscript are not significantly different.

Site	Control		Acidified		p_{ANOVA}	p_{ANOVA}	p_{ANOVA}
Species	***Paracentrotus lividus***	***Arbacia lixula***	***Paracentrotus lividus***	***Arbacia lixula***	**species**	**sites**	**species*sites**
pH_T (total scale)	7.50 ± 0.17 [a]	7.10 ± 0.22 [b]	7.47 ± 0.08 [a]	7.14 ± 0.15 [b]	**$<10^{-3}$**	0.802	0.474
TA (µmolkg-1)	3845 ± 215 [a]	2575 ± 597 [b]	4338 ± 615 [a]	2336 ± 702 [b]	**$<10^{-3}$**	0.683	0.250
DIC (mM)	3.83 ± 0.64 [a]	2.84 ± 0.52 [b]	4.18 ± 1.05 [a]	2.65 ± 0.31 [b]	**$<10^{-3}$**	0.751	0.289
pCO_2 (µatm)	2933 ± 1243 [b]	5283 ± 2498 [a]	3253 ± 1366 [b]	4185 ± 1694 [a]	**0.009**	0.513	0.238
$[HCO_3^-]$ (mM)	3514 ± 591 [a]	2575 ± 501 [b]	3848 ± 969 [a]	2421 ± 274 [b]	**$<10^{-3}$**	0.698	0.297
$[CO_3^{2-}]$ (mM)	137 ± 61 [a]	42 ± 20 [b]	132 ± 27 [a]	43 ± 12 [b]	**$<10^{-3}$**	0.889	0.829
$\delta^{13}C$	-5.34 ± 0.70 [a]	-4.08 ± 2.40 [a]	-5.74 ± 1.66 [b]	-6.52 ± 2.05 [b]	0.693	**0.027**	0.106
Ω Calcite	3.23 ± 1.43 [a]	1.00 ± 0.47 [b]	3.12 ± 0.63 [a]	1.02 ± 0.28 [b]	**$<10^{-3}$**	0.894	0.843
Ω Aragonite	2.13 ± 0.95 [a]	0.66 ± 0.31 [b]	2.06 ± 0.41 [a]	0.68 ± 0.19 [b]	**$<10^{-3}$**	0.891	0.832
Diameter (mm)	39.4 ± 4.4 [a,b]	35.9 ± 4.8 [b,c]	42.4 ± 3.8 [a]	32.8 ± 2.1 [c]	**$<10^{-3}$**	0.968	**0.018**
Height test (mm)	22.1 ± 2.5 [a]	17.7 ± 6.9 [b]	24.6 ± 2.5 [a]	16.0 ± 3.3 [b]	**$<10^{-3}$**	0.764	0.121

Table 4. Characteristic stress (σ_0) and Weibull modulus and their 95% confidence intervals, of ambital plates of the test of the sea urchins *P. lividus* and *A. lixula* at control and acidified sites at Levante Bay analysed with Weibull probabilistic method following Butikofer et al. 2015

Species	Site	n_σ	Weibull modulus (m)	m $CI_{95\%}$ -	m $CI_{95\%}$ +	σ_0 (MPa)	σ_0 (MPa) $CI_{95\%}$ -	σ_0 (MPa) $CI_{95\%}$ +
P. lividus	Control	49	1.455	1.085	1.951	417.72	339.27	514.31
A. lixula		47	1.362	1.009	1.838	555.75	442.97	697.26
P. lividus	Acidified	47	1.452	1.075	1.959	363.67	293.94	449.94
A. lixula		49	1.896	1.414	2.544	323.25	275.57	379.17

Table 5. Characteristic force at fracture (F_{max0}) and characteristic Young's modulus (E_0) ant their 95% confidence intervals of the ambital and apical plates of the test and the spines of the sea urchins *P. lividus* and *A. lixula* at control and acidified sites at Levante Bay analysed with Weibull probabilistic method following Butikofer et al. 2015

Ambital plates									
Species	site	n_{Fmax}	F_{max0} (N)	F_{max0} (N) $CI_{95\%}$ -	F_{max0} (N) $CI_{95\%}$ +	n_E	E_0(GPa)	E_0 (GPa) $CI_{95\%}$ -	E_0 (GPa) $CI_{95\%}$ +
P. lividus	Control	50	6.66	6.06	7.32	49	46.09	37.73	56.30
A. lixula		49	7.47	6.85	8.14	47	58.21	46.87	72.29
P. lividus	Acidified	50	6.67	5.99	7.43	47	42.22	34.14	52.20
A. lixula		50	6.10	5.69	6.55	49	30.14	25.89	35.07
Apical plates									
Species	site	n_{Fmax}	F_{max0} (N)	F_{max0} (N) $CI_{95\%}$ -	F_{max0} (N) $CI_{95\%}$ +	n_E	E_0(GPa)	E_0 (GPa) $CI_{95\%}$ -	E_0 (GPa) $CI_{95\%}$ +
P. lividus	Control	47	26.19	23.97	28.61	46	1.61	1.24	2.09
A. lixula		50	30.98	28.62	33.53	50	1.61	1.24	2.10
P. lividus	Acidified	50	23.30	21.75	24.96	50	1.26	1.09	1.45
A. lixula		50	30.47	28.26	32.84	50	1.54	1.14	2.09
Spines									
Species	site	n_{Fmax}	F_{max0} (N)	F_{max0} (N) $CI_{95\%}$ -	F_{max0} (N) $CI_{95\%}$ +	n_E	E_0(GPa)	E_0 (GPa) $CI_{95\%}$ -	E_0 (GPa) $CI_{95\%}$ +
P. lividus	Control	49	1.39	1.28	1.51	44	86.80	65.14	115.67
A. lixula		49	1.31	1.19	1.44	47	90.05	78.58	103.20
P. lividus	Acidified	48	1.22	1.12	1.34	46	71.18	59.08	85.75
A. lixula		43	1.07	0.99	1.16	42	67.54	59.41	76.79

Table 6. Characteristic nanoelasticity (E_0) and characteristic nanohardness (H_0) and their 95% confidence intervals of the ambital plates of the test and of the spines of the sea urchins *P.*

lividus and *A. lixula* at control and acidified sites at Levante Bay analysed with Weibull probabilistic method following Butikofer et al. 2015

Ambital plates									
Species	Site	n_E	E_0(GPa)	E_0 (GPa) $CI_{95\%}$ -	E_0 (GPa) $CI_{95\%}$ +	n_H	H_0(GPa)	H_0 (GPa) $CI_{95\%}$ -	H_0 (GPa) $CI_{95\%}$ +
P. lividus	Control	84	58.74	56.14	61.45	82	4.69	4.41	4.99
A. lixula		92	60.35	57.72	63.10	91	4.77	4.47	5.10
P. lividus	Acidified	50	55.64	52.51	58.97	48	4.65	4.35	4.97
A. lixula		61	55.06	52.03	58.27	61	4.44	4.08	4.83
Spines									
Species	Site	n_E	E_0(GPa)	E_0 (GPa) $CI_{95\%}$ -	E_0 (GPa) $CI_{95\%}$ +	n_H	H_0(GPa)	H_0 (GPa) $CI_{95\%}$ -	H_0 (GPa) $CI_{95\%}$ +
P. lividus	Control	105	67.61	65.38	69.92	102	5.02	4.84	5.21
A. lixula		74	59.36	56.61	62.24	74	4.43	4.13	4.74
P. lividus	Acidified	98	66.15	64.08	68.28	99	5.09	4.85	5.34
A. lixula		50	56.11	53.16	59.21	51	4.56	4.23	4.92

Supplementary Materials

Are control of extracellular acid-base balance and regulation of skeleton genes linked to resistance to ocean acidification in adult sea urchins?

Di Giglio S.[1], Spatafora D.[2], Milazzo M.[2], M'Zoudi S.[1], Zito. F.[3], Dubois Ph. [1]*, Costa C.* [3]

S01. Preliminary settings for Real Time qPCR Comparative Assays

- Target genes description

The genes whose expression has been analysed in this work have been well characterized and their role is known in different sea urchin species. They were selected based on the literature summarized below. Mann et al. (2008) found that the organic matrix from adult sea urchin skeleton includes several C-type lectins, metalloproteases, small acidic proteins, collagens and enzymes such as carbonic anhydrase. In *P. lividus*, Karakostis et al. (2016a) characterized *Pl-can*, a component of the sea urchin carbonic anydrases family specifically expressed in the primary mesenchymal cells (PMCs) of the embryos, which mainly ensures the transport of bicarbonate ions and it is likely involved in biomineral remodelling. The PMC-specific cell surface glycoprotein, MSP130, is thought to be involved in the binding and sequestration of Ca^{2+} ions for subsequent deposition into the growing skeleton (Anstrom et al., 1987; Farach-Carson et al., 1989; Illies et al., 2002; Leaf et al., 1987). SM50, a PMC-specific lectin protein with a basic isoelectric point (pI), has been first identified in *S. purpuratus* embryos by Sucov et al. (1987) and subsequently was found in an organic layer surrounding calcitic elements, localized in pedicellaria, test and teeth of adult *P. lividus* by Ameye et al. (1999). Its glycine rich domain is thought to mediate the amorphous calcium carbonate (ACC) stabilization and to direct the calcite polymorph formation (Jain et al., 2017). P19, is an mRNA expressed in PMC of *P. lividus* embryos (Costa et al., 2012), it encodes for an acidic protein rich in glutamic acid. The adult protein identified in homologous sea urchins species has been hypothesized to have different functions, including

the mechanical strengthening of calcite plates due to the high magnesium content (Alvares et al., 2009).

- Sequences selection, primer design, One Step RT-PCR and amplicons validation

The sea urchin biomineralization genes *p19, msp130, sm50, can* as well as the potential reference *z12-1* gene were selected to analyze the expression profiles in both species by qPCR. An *in silico* analysis was performed and all mRNA sequences were firstly searched at the NCBI's nucleotide database (https://www.ncbi.nlm.nih.gov/pubmed/). Six sequences were retrieved, *z12.1* (LT900344.1), *p19* (FR693764), *sm50* (AJ515510), *can* (HG422057.1) of *P. lividus and msp130* (NM_001123514.1, KY234302.1) of *S. purpuratus* and *A. lixula,* respectively. Then, a TBLASTN search was performed on *P. lividus* and *A. lixula* databases at the website http://octopus.obs-vlfr.fr/blast/oursin/blast_oursin.php. (restricted access, *P. lividus* genome project), in order to retrieve the other selected sequences from both species. The identified sequences were translated and their homology degree was further evaluated by aligning with known proteins from other sea urchin species, by using LALIGN and local alignment method at the https://www.expasy.org/ website. Specific primer pairs to be used in qPCR comparative assays were designed by using Primer Express software (version 2.0.0, Applied Biosystems, Foster City, CA, USA) (Table S01.1.) and purchased from Invitrogen through BMR Genomics service (Padova - Italy). The sequences that were not found by *in silico* analysis were amplified using primers of orthologous sequences. In order to validate primers pairs but also to evaluate the tissue to use in this study, preliminary amplification reactions were performed on total RNA by using One Step RT-PCR following the manufacturer's instructions (Invitrogen by Life technologies) with some modifications as described in Costa et al. (2019). Single amplicons from each reaction visualized on 2% agarose gels were cloned in pGEM T Easy vector (Promega, Madison, WI, USA) and bi-directionally sequenced using BMR

Genomics service (Padova - Italy), in order to validate the amplicons (Table S01.1.). The sequences, here identified for the first time, were submitted to NCBI GenBank obtaining the accession numbers: MN917142, MN917143, MN917144, MN917145 and MN938929 respectively for *Al*-z12.1, *Al*-p19, *Al*-sm50, *Al*-can and *Pl*-msp130.

- Identification of mRNA sequences

To analyze the expression of biomineralization-related genes in specimens of *P. lividus* and *A. lixula* from acidified and control sites, by qPCR, *p19, msp130, sm50* and *can* target genes were chosen for both species, along with a potential reference gene, such as *z12-1,* used in *P. lividus* embryos gene expression analyses, in different experimental conditions (Costa et al. 2012). Apart the known *Pl-z12.1*, *Pl-p19*, *Pl-sm50*, *Pl-can*, *Al-msp130* mRNA sequences retrieved at NCBI database, the putative *Al-z12-1, Al-p19* and *Pl*-msp130 mRNAs were identified in the transcriptome databases of *A. lixula* and *P. lividus*, respectively, for their high homology degree with known orthologs. In particular, using the known *Pl-Z12.1* protein sequence (A. Number: LT900344.1), two highly similar *z12-1* partial mRNA sequences (99.7 %) for *A. lixula* were identified. The longest one, lacking a 5'coding sequence (CDS) part, translated a deduced partial sequence of 503 amino acid (aa) that showed high identities (58.7 % and 62.1 %) and high similarities (78.7 % and 80.3 %) with both *P. lividus* and *S. purpuratus* proteins sequences, respectively (A. Numbers: SNT86442.1 and NP_999781.1). Using the known 165aa *Pl*-P19 protein (A. Number: CBX24531.1), an mRNA sequence that translated a 170aa protein was intercepted, highly homologous to *Pl*-P19, with which it shared 71.9% of identity and 85.4% of similarity. In further alignments, it showed high identities (76.3% and 74.4%) and similarities (85.0% and 87.8%), with the 166aa P19L of *S. purpuratus* (A. Number: NP_999812.) and 166aa P19 tooth matrix protein of *Lytechinus variegatus* (A. Number: ACU00092.1), respectively. Regarding *Pl*-msp130 mRNA, the TBLASTN search using the

805aa *Sp*-MSP130 protein (A. Number: NP 00116986.1) hit a *P. lividus* mRNA coding for a putative 881aa *Pl*-MSP130. This showed 70.1%, 68.2% and 66.9% high identities, and 80.7%, 78.0% and 78.4% high similarities with orthologs of *S. purpuratus* 805aa (A. Number: NP 00116986.1), *Holothuria tuberculata* 781aa (A. Number: CAC20589) and *Hemicentrotus erythrogramma* 774aa (A. Number: CAC20358.1), respectively. Specifc primers designed on the identified *Al-z12.1*, *Al-p19* and *Pl-msp130* sequences, in preliminary One Step RT-PCR, produced amplicons corresponding to the expected regions, as confirmed by cloning and sequencing (Table 1 and S01.1.). Differently, our investigations did not produce results for *Al-sm50* and *Al-can*, due to the lack of *A. lixula* skeleton transcriptome. On the contrary, amplification reactions performed on *A. lixula* total RNA using oligo couples designed on the respective *P. lividus* sequences, produced amplicons highly homologous to sea urchin *sm50* and *can* genes, confirming their new identification.

Table S01.1. Amplicon sequences from One Step RT-PCR

Pl-z12.1
AGCGCCACACCAAAAGAAGTCAACTAACCATGTCTTTCAGTACGATGCTCATCAT
GACATCCCCTTCAGTCCAAACAGCCCTGTCTATCATCC 93bp

Pl-p19
GCAGGAGACTAAGACAGAGACTGCACCCGAAGCACCACCTAAGACTGACCCCGA
GGCCAAGGTCGAAGGAGAGGC GAGCGGAG 83bp

Pl-msp130
GTTGACCCCGTAACCATGAACGCCACCTTGGCCTGGGACAGCGGTGACGTCATCG
AGAAGGAGGTTGCAAAGTTCTTCCC 80bp

Pl-sm50
CCGTGAACGCACAAAATCCCCTTGCACCCGCACCAGGATCGGCTCCAGTCATGAA
GCGTCCGGG 64bp

Pl-can
CCAAAATGCTGGGAAAGTGTAACATGGTCGGTCGGCTGCAATCCAATTCATCTTT
CACATAATCAGCTTGACATGTTCCGA 81bp

Al-Z12.1
GTCTGCCTGAAGACCTTCGCACAGAAGTGCGACCTCACGCGCCACATCCGCACAC
ACACGGGCGAGAAACCGCACGAGTGCGAGGAATGCGGGAAGTCTTTC 102bp

Al-p19
GAGAGCACGAGAGGGGAACAGCGTGAAGGGGCAGAGCGGTGCTTGCACAGAGG
CGGCAAACTCAGGAGAGGACAGGCAGCCAACGGAGGCTGAGATGGACGC 102
bp

Al-msp130
GGGTCCTGAGTGCGAGTCTCTCGCAGTGGGCGACGTCCAGGGCCGTAAGCTCATC
TTCGTCGGCATCGACGGCGTCA GCGCTCTCGCCATC 91bp

Al-sm50
CCGTGAACGCACAAAATCCCCTTGCACCGGCTCCAGGCTCCGGACCAGTCATGAA
GCGTCCGGG 64bp

Al-can
CCAAAATGCTGGGAAAGTGTAACATGGTCGGTTGGCTGTAATGTAATCCACCTTT
CACATAATCAGCTTGACATGTTCCGA 81bp

Table S01.2. Cycle threshold (CT) values of the housekeeping gene z12-1 in *P. lividus* and *A. lixula* from control and acidified site. CT were tested with one-factor repeated ANOVA (site: fixed factor, repeated factor: qPCR assay, n=5) for each species separately.

Species	Site	Threshold cycle (N°)		p_{ANOVA}
P. lividus	Control	29.311	± 0.900	0.289
	Acidified	29.959	± 0.912	
A. lixula	Control	28.310	± 1.350	0.367
	Acidified	27.284	± 2.059	

S02. Results of ANOVA model I (site: fixed factor) on chemical parameters of sea water from control and acidified site at Levante Bay, Vulcano

	Mann-Whitney U test Statistic	Chi-square approximation	df	p-value
pH_T	0.000	3.857	1	**0.049**
TA	4.000	0.0476	1	0.827
DIC	9.000	3.857	1	**0.049**
pCO_2	9.000	3.857	1	**0.049**
$[HCO_3^-]$	9.000	3.857	1	**0.049**
$[CO_3^{2-}]$	0.000	3.857	1	**0.049**
ΩCa	0.000	3.970	1	**0.046**
ΩAr	0.000	3.857	1	**0.049**
$\delta^{13}C$	5.000	0.048	1	0.827

S03. Results of two-factor ANOVA (species: fixed factor, site: crossed fixed factor) on chemical parameters of the coelomic fluid of *Arbacia lixula* and *Paracentrotus lividus* from control and acidified sites at Levante Bay, Vulcano

	Factor	Sum of squares	Numerator df	Denominator df	Mean square	F-ratio	p_{ANOVA}
pH_T	Site	0.002	1	36	0.002	0.064	0.802
	Species	1.334	1	36	1.338	51.685	**$<10^{-3}$**
	Site*Species	0.014	1	36	0.014	0.525	0.474
	Error	0.929	36		0.026		
TA	Site	6.22E+04	1	12	6.22E+04	0.175	0.683
	Species	1.04E+07	1	12	1.04E+07	29.109	**$<10^{-3}$**
	Site*Species	5.19E+05	1	12	5.19E+05	1.459	0.250
	Error	4.27E+06	12		3.56E+05		
DIC	Site	0.053	1	30	0.053	0.102	0.751
	Species	13.269	1	30	13.269	25.754	**$<10^{-3}$**
	Site*Species	0.599	1	30	0.599	1.163	0.289
	Error	15.457	30				
pCO_2	Site	5.72E+05	1	12	5.72E+05	0.400	0.539
	Species	4.10E+05	1	12	4.10E+05	0.287	0.602
	Site*Species	7.90E+05	1	12	7.90E+05	0.552	0.472
	Error	1.72E+07	12		1.43E+06		
$[HCO_3^-]$	Site	8.83E+04	1	12	8.83E+04	0.277	0.608
	Species	8.08E+06	1	12	8.08E+06	25.333	**$<10^{-3}$**
	Site*Species	5.45E+05	1	12	5.45E+05	1.710	0.216
	Error	3.83E+06	12		3.19E+05		
$[CO_3^{2-}]$	Site	368.173	1	12	368.173	0.366	0.557
	Species	29970.902	1	12	29970.902	29.769	**$<10^{-3}$**
	Site*Species	42.914	1	12	42.914	0.043	0.840
	Error	12081.421	12		1006.785		
Ωcalcite	Site	0.211	1	12	0.211	0.376	0.551
	Species	16.747	1	12	16.747	29.866	**$<10^{-3}$**
	Site*Species	0.026	1	12	0.026	0.047	0.832
	Error	6.729	12		0.561		
Ωaragonite	Site	0.088	1	12	0.088	0.357	0.561
	Species	7.299	1	12	7.299	29.699	**$<10^{-3}$**
	Site*Species	0.011	1	12	0.011	0.044	0.838
	Error	2.949	12		0.246		
$\delta^{13}C$	Site	16.843	1	30	16.843	5.440	**0.027**
	Species	0.491	1	30	0.491	0.159	0.693
	Site*Species	8.591	1	30	8.591	2.775	0.106
	Error	92.891	30		3.096		
D	Site	0.025	1	36	0.025	0.002	0.968
	Species	429.025	1	36	429.025	28.220	**$<10^{-3}$**
	Site*Species	93.025	1	36	93.003	6.119	**0.018**
	Error	547.300	36		15.203		
H	Site	1.600	1	36	1.600	0.092	0.764
	Species	422.500	1	36	422.500	2.417	**$<10^{-3}$**
	Site*Species	44.100	1	36	44.100	2.522	0.121
	Error	629.400	36		629.400		

S04. Mechanical and morphometric properties of the ambital and apical plates of the test and the spines of the sea urchins *P. lividus* and *A. lixula* at control and acidified sites (Mean ± SD, n=10) at Levante Bay.

Ambital plates				
Site	**Control**		**Acidified**	
Species	***P. lividus***	***A. lixula***	***P. lividus***	***A. lixula***
n individuals	10	10	10	10
F_{max} (N)	5.96 ± 1.71	6.69 ± 1.83	5.94 ± 2.08	5.55 ± 0.94
I_2 (10^{-14} m^4)	2.89 ± 1.03	2.85 ± 1.83	3.39 ± 1.44	2.72 ± 1.30
Effective length L_e (mm)	7.46 ± 0.95	7.76 ± 1.33	7.93 ± 0.70	7.11 ± 0.70
Thickness H (mm)	0.53 ± 0.07	0.60 ± 0.06	0.56 ± 0.07	0.56 ± 0.08
Young's modulus E (GPa)	41.80 ± 14.95	51.82 ± 18.60	38.93 ± 14.15	26.69 ± 8.43
Stress σ (MPa)	384 ± 194	498 ± 202	342 ± 186	285 ± 74
Flexural stiffness (EI_2) (10^{-4} Nm^2)	8.44 ± 3.54	9.74 ± 5.09	8.95 ± 3.28	5.65 ± 1.47
Apical plates				
F_{max} (N)	23.73 ± 4.44	28.01 ± 5.58	21.25 ± 2.89	27.61 ± 4.05
Effective length L_e (mm)	2.85 ± 0.45	3.06 ± 0.37	2.71 ± 0.22	3.07 ± 0.41
F_{max}/L_e (Nm^{-1})	8.17 ± 2.55	9.46 ± 1.63	8.25 ± 1.27	9.27 ± 2.01
Thickness H (mm)	1.20 ± 0.07	1.17 ± 0.14	1.15 ± 0.08	1.14 ± 0.06
Young's modulus E (GPa)	1.60 ± 1.36	1.53 ± 0.95	1.12 ± 0.31	1.68 ± 1.35
Spines				
F_{max} (N)	1.25 ± 0.15	1.18 ± 0.17	1.08 ± 0.26	0.98 ± 0.13
Effective length L_e (mm)	12.89 ± 2.57	14.39 ± 2.30	10.86 ± 2.03	14.03 ± 2.77
F_{max}/L_e (Nm^{-1})	96.83 ± 22.18	77.58 ± 14.97	96.16 ± 22.65	68.15 ± 15.97
Young's modulus E (GPa)	75.55 ± 26.55	80.09 ± 17.37	61.16 ± 23.11	60.27 ± 18.76

S05. Weibull calculation of 95% confidence intervals according to Butikofer et al. 2015. mhat ($\widehat{m}$) and shat ($\widehat{s}$) are estimates for m (Weibull modulus) and σ_0, F_{max0}, E_0 (characteristic strength, F_{max}, Young's modulus) of ambital plates, respectively. m $CI_{95\%}$ - and + : lower and upper limits of 95% confidence interval on m (Weibull modulus) value and σ_0, F_{max0}, E_0 $CI_{95\%}$ - and +: lower and upper limits of 95% confidence interval on characteristic strength, F_{max}, Young's modulus of ambital plates, respectively.

Stress σ (Pa)													
Species	**sites**	**n**	**m**	**c**	**R²**	**p-value**	**σ_0 (MPa)**	**mhat**	**m $CI_{95\%}$ -**	**m $CI_{95\%}$ +**	**shat**	**σ_0 (MPa) $CI_{95\%}$ -**	**σ_0 (MPa) $CI_{95\%}$ +**
P. lividus	Control	49	1.455	-8.779	0.928	$<10^{-3}$	417.72	1.455	1.085	1.951	418	339	514
A. lixula	Control	47	1.362	-8.609	0.992	$<10^{-3}$	555.75	1.362	1.009	1.838	556	443	697
P. lividus	Acidified	47	1.452	-8.559	0.898	$<10^{-3}$	363.67	1.452	1.075	1.959	364	294	450
A. lixula	Acidified	49	1.896	-10.958	0.945	$<10^{-3}$	323.25	1.896	1.414	2.544	323	276	380
Fmax (N)													
Species	**sites**	**n**	**m**	**c**	**R²**	**p-value**	**F_{max0} (N)**	**mhat**	**m $CI_{95\%}$ -**	**m $CI_{95\%}$ +**	**shat**	**F_{max0} (N) $CI_{95\%}$ -**	**F_{max0} (N) $CI_{95\%}$ +**
P. lividus	Control	50	3.184	-6.038	0.942	$<10^{-3}$	6.662	3.184	2.381	4.258	6.662	6.064	7.319
A. lixula	Control	49	3.523	-7.083	0.960	$<10^{-3}$	7.466	3.523	2.627	4.726	7.466	6.851	8.135
P. lividus	Acidified	50	2.771	-5.259	0.834	$<10^{-3}$	6.669	2.771	2.072	3.706	6.669	5.986	7.430
A. lixula	Acidified	50	4.244	-7.675	0.874	$<10^{-3}$	6.101	4.244	3.173	5.675	6.101	5.686	6.548
Young's Modulus E (GPa)													
Species	**sites**	**n**	**m**	**c**	**R²**	**p-value**	**E_0(GPa)**	**mhat**	**m $CI_{95\%}$ -**	**m $CI_{95\%}$ +**	**shat**	**E_0 (GPa) $CI_{95\%}$ -**	**E_0 (GPa) $CI_{95\%}$ +**
P. lividus	Control	49	1.512	-37.116	0.951	$<10^{-3}$	46.09	1.51	1.13	2.03	4.61E+10	37.73	56.30
A. lixula	Control	47	1.426	-35.350	0.987	$<10^{-3}$	58.21	1.43	1.06	1.92	5.82E+10	46.87	72.29
P. lividus	Acidified	47	1.456	-35.620	0.928	$<10^{-3}$	42.22	1.46	1.08	1.96	4.22E+10	34.14	52.20
A. lixula	Acidified	49	1.994	-48.121	0.965	$<10^{-3}$	30.14	1.99	1.49	2.68	3.01E+10	25.89	35.07
Fmax/Le (N/m)													
Species	**sites**	**n**	**m**	**c**	**R²**	**p-value**	**F_{max}/L_{e0}**	**mhat**	**m $CI_{95\%}$ -**	**m $CI_{95\%}$ +**	**shat**	**F_{max}/L_{e0} $CI_{95\%}$ -**	**F_{max}/L_{e0} $CI_{95\%}$ +**
P. lividus	Control	50	2.967	-20.226	0.942	$<10^{-3}$	913	2.97	2.22	3.97	913	825	1011
A. lixula	Control	49	3.008	-20.819	0.960	$<10^{-3}$	1013	3.01	2.24	4.04	1013	916	1120
P. lividus	Acidified	50	2.688	-18.132	0.834	$<10^{-3}$	851	2.69	2.01	3.59	851	761	951
A. lixula	Acidified	50	3.836	-25.987	0.874	$<10^{-3}$	876	3.84	2.87	5.13	876	810	947

S06. Weibull calculation of 95% confidence intervals according to Butikofer et al. 2015. mhat ($\widehat{m}$) and shat $(\widehat{s})$ are estimates for m (Weibull modulus) and F_{max0}, E_0 (characteristic F_{max}, Young's modulus) of apical plate. m $CI_{95\%}$ - and +: lower and upper limits of 95% confidence interval on m (Weibull modulus) value and F_{max0}, E_0 $CI_{95\%}$ - and +: lower and upper limits of 95% confidence interval on characteristic F_{max} and Young modulus of apical plates.

F_{max} (N)													
Species	**sites**	**n**	**m**	**c**	**R²**	**p-value**	**F_{max0} (N)**	**mhat**	**m $CI_{95\%}$ -**	**m $CI_{95\%}$ +**	**shat**	**F_{max0} (N) $CI_{95\%}$ -**	**F_{max0} (N) $CI_{95\%}$ +**
P. lividus	Control	47	3.499	-11.424	0.957	$<10^{-3}$	26.188	3.499	2.592	4.722	26.188	23.974	28.606
A. lixula	Control	50	3.783	-12.989	0.956	$<10^{-3}$	30.981	3.783	2.829	5.060	30.981	28.622	33.534
P. lividus	Acidified	50	4.35	-13.71	0.96	$<10^{-3}$	23.30	4.35	3.26	5.82	23.30	21.75	24.96
A. lixula	Acidified	50	3.99	-13.64	0.97	$<10^{-3}$	30.47	3.99	2.98	5.34	30.47	28.26	32.84
Young's Modulus E (GPa)													
Species	**sites**	**n**	**m**	**c**	**R²**	**p-value**	**E_0(GPa)**	**mhat**	**m $CI_{95\%}$ -**	**m $CI_{95\%}$ +**	**shat**	**E_0 (GPa) $CI_{95\%}$ -**	**E_0 (GPa) $CI_{95\%}$ +**
P. lividus	Control	46	1.20	-25.34	0.80	$<10^{-3}$	1.61	1.20	0.88	1.62	1.61E+09	1.24	2.09
A. lixula	Control	50	1.13	-23.97	0.89	$<10^{-3}$	1.61	1.13	0.85	1.51	1.61E+09	1.24	2.10
P. lividus	Acidified	50	2.13	-44.68	0.97	$<10^{-3}$	1.26	2.13	1.59	2.85	1.26E+09	1.09	1.45
A. lixula	Acidified	50	0.98	-20.78	0.92	$<10^{-3}$	1.54	0.98	0.73	1.31	1.54E+09	1.14	2.09
F_{max}/L_e (N/m)													
Species	**sites**	**n**	**m**	**c**	**R²**	**p-value**	**F_{max}/L_{e0}**	**mhat**	**m $CI_{95\%}$ -**	**m $CI_{95\%}$ +**	**shat**	**F_{max}/L_{e0} $CI_{95\%}$ -**	**F_{max}/L_{e0} $CI_{95\%}$ +**
P. lividus	Control	46	2.534	-23.344	0.957	$<10^{-3}$	1.00E+04	2.53	1.87	3.43	1.00E+04	8.87E+03	1.13E+04
A. lixula	Control	50	3.517	-32.576	0.956	$<10^{-3}$	1.05E+04	3.52	2.63	4.70	1.05E+04	9.67E+03	1.15E+04
P. lividus	Acidified	50	3.121	-28.491	0.964	$<10^{-3}$	9.22E+03	3.12	2.33	4.17	9.22E+03	8.38E+03	1.02E+04
A. lixula	Acidified	50	3.716	-34.318	0.974	$<10^{-3}$	1.03E+04	3.72	2.78	4.97	1.03E+04	9.47E+03	1.11E+04

S07. Weibull calculation of 95% confidence interval according to Butikofer et al. 2015. mhat ($\widehat{m}$) and shat ($\widehat{(s)}$) are estimates for m (Weibull modulus) and F_{max0}, E_0 (characteristic F_{max}, Young's modulus) of spines. m $CI_{95\%}$ - and +: lower and upper limits of 95% confidence interval on m (Weibull modulus) value and F_{max0}, E_0 $CI_{95\%}$ - and +: lower and upper limits of 95% confidence interval on characteristic F_{max} and Young's modulus of spines.

F_{max} (N)													
Species	**sites**	**n**	**m**	**c**	**R^2**	**p-value**	**F_{max0} (N)**	**mhat**	**m $CI_{95\%}$ -**	**m $CI_{95\%}$ +**	**shat**	**F_{max0} (N) $CI_{95\%}$ -**	**F_{max0} (N) $CI_{95\%}$ +**
P. lividus	Control	49	3.711	-1.224	0.935	$<10^{-3}$	1.391	3.711	2.767	4.978	1.391	1.282	1.509
A. lixula	Control	49	3.106	-0.839	0.970	$<10^{-3}$	1.310	3.106	2.316	4.166	1.310	1.188	1.444
P. lividus	Acidified	48	3.365	-0.680	0.986	$<10^{-3}$	1.224	3.365	2.501	4.527	1.224	1.118	1.340
A. lixula	Acidified	43	4.113	-0.282	0.980	$<10^{-3}$	1.071	4.113	3.007	5.628	1.071	0.990	1.159
Young's Modulus E (GPa)													
Species	**sites**	**n**	**m**	**c**	**R^2**	**p-value**	**E_0(GPa)**	**mhat**	**m $CI_{95\%}$ -**	**m $CI_{95\%}$ +**	**shat**	**E_0 (GPa) $CI_{95\%}$ -**	**E_0 (GPa) $CI_{95\%}$ +**
P. lividus	Control	44	1.112	-28.010	0.899	$<10^{-3}$	86.80	1.112	0.816	1.516	86.80	65.14	115.67
A. lixula	Control	47	2.267	-57.174	0.918	$<10^{-3}$	90.05	2.267	1.679	3.059	90.05	78.58	103.20
P. lividus	Acidified	46	1.676	-41.892	0.897	$<10^{-3}$	71.18	1.676	1.238	2.270	71.18	59.08	85.75
A. lixula	Acidified	42	2.547	-63.510	0.859	$<10^{-3}$	67.54	2.547	1.855	3.498	67.54	59.41	76.79
F_{max}/L_e (N/m)													
Species	**sites**	**n**	**m**	**c**	**R^2**	**p-value**	**F_{max}/L_{e0}**	**mhat**	**m $CI_{95\%}$ -**	**m $CI_{95\%}$ +**	**shat**	**F_{max}/L_{e0} $CI_{95\%}$ -**	**F_{max}/L_{e0} $CI_{95\%}$ +**
P. lividus	Control	49	2.808	-13.198	0.935	$<10^{-3}$	110	2.81	2.09	3.77	110	99	122
A. lixula	Control	49	2.697	-12.036	0.970	$<10^{-3}$	87	2.70	2.01	3.62	87	77	967
P. lividus	Acidified	48	3.010	-14.119	0.986	$<10^{-3}$	109	3.01	2.24	4.05	109	98	121
A. lixula	Acidified	43	3.044	-13.181	0.980	$<10^{-3}$	76	3.04	2.23	4.17	76	68	84

S08. Nanoelasticity and nanohardness of the ambital plates of the test and of the spines of the sea urchins *P. lividus* and *A. lixula* from control and acidified sites (Mean ± SD, n=5) at Levante Bay measured by nanoindentation.

Ambital plates				
Sites	**Control**		**Acidified**	
Species	***P. lividus***	***A. lixula***	***P. lividus***	***A. lixula***
Young's modulus (E) (GPa)	53.57 ± 5.75	54.63 ± 2.19	49.90 ± 3.77	50.10 ± 7.31
Hardness (GPa)	4.24 ± 0.72	4.01 ± 0.61	4.22 ± 0.29	4.00 ± 0.77
Spines				
Sites	**Control**		**Acidified**	
Species	***P. lividus***	***A. lixula***	***P. lividus***	***A. lixula***
Young's modulus (E) (GPa)	62.54 ± 8.59	53.20 ± 5.94	61.16 ± 5.57	52.18 ± 5.95
Hardness (GPa)	4.63 ± 0.55	3.93 ± 0.27	4.59 ± 0.64	4.19 ± 0.35

S09. Weibull calculation of 95% confidence intervals according to Butikofer et al. 2015. mhat ($\widehat{m}$) and shat ($\widehat{(s)}$) are estimates for nanohardness (H_0 : characteristic nanohardness) and nanoelasticity (E_0 characteristic nanoelasticity) of the ambital plates and the spines. m $CI_{95\%}$- and +: lower and upper limits of 95% confidence intervals on m (Weibull modulus) value and H_0, E_0 $CI_{95\%}$ - and +: lower and upper limits of 95% confidence intervals on characteristic nanohardness and nanoelasticity of the ambital plates and the spines.

Ambital plates													
Nanohardness													
Species	**site**	**n**	**m**	**c**	**R²**	**p-value**	**H_0(GPa)**	**mhat**	**m $CI_{95\%}$ -**	**m $CI_{95\%}$ +**	**shat**	**H_0 (GPa) $CI_{95\%}$ -**	**H_0 (GPa) $CI_{95\%}$ +**
P. lividus	Control	82	3.781	-5.845	0.899	$< 10^{-3}$	**4.69**	3.781	3.013	4.745	4.69	**4.41**	**4.99**
A. lixula		91	3.384	-5.289	0.958	$< 10^{-3}$	**4.77**	3.384	2.728	4.197	4.77	**4.47**	**5.10**
P. lividus	Acidified	48	4.568	-7.018	0.885	$< 10^{-3}$	**4.65**	4.568	3.395	6.145	4.65	**4.35**	**4.97**
A. lixula		61	3.220	-4.799	0.924	$< 10^{-3}$	**4.44**	3.220	2.475	4.190	4.44	**4.08**	**4.83**
Nanoelasticity E (GPa)													
Species	**site**	**n**	**m**	**c**	**R²**	**p-value**	**E_0(GPa)**	**mhat**	**m $CI_{95\%}$ -**	**m $CI_{95\%}$ ++**	**shat**	**E_0 (GPa) $CI_{95\%}$ -**	**E_0 (GPa) $CI_{95\%}$ +**
P. lividus	Control	84	5.113	-20.825	0.894	$< 10^{-3}$	**58.74**	5.113	4.086	6.398	58.74	**56.14**	**61.45**
A. lixula		92	4.951	-20.298	0.955	$< 10^{-3}$	**60.35**	4.951	3.996	6.134	60.35	**57.72**	**63.10**
P. lividus	Acidified	50	5.164	-20.756	0.887	$< 10^{-3}$	**55.64**	5.164	3.862	6.907	55.64	**52.51**	**58.97**
A. lixula		61	4.792	-19.207	0.922	$< 10^{-3}$	**55.06**	4.792	3.683	6.234	55.06	**52.03**	**58.27**
Spines													
Nanohardness													
Species	**site**	**n**	**m**	**c**	**R²**	**p-value**	**H_0(GPa)**	**mhat**	**m $CI_{95\%}$ -**	**m $CI_{95\%}$ +**	**shat**	**H_0 (GPa) $CI_{95\%}$ -**	**H_0 (GPa) $CI_{95\%}$ +**
P. lividus	Control	102	5.660	-9.136	0.990	$< 10^{-3}$	**5.02**	5.660	4.618	6.938	5.02	**4.84**	**5.21**
A. lixula		70	3.542	-5.231	0.990	$< 10^{-3}$	**4.38**	3.542	2.771	4.529	4.38	**4.08**	**4.70**
P. lividus	Acidified	99	4.456	-7.248	0.978	$< 10^{-3}$	**5.09**	4.456	3.624	5.479	5.09	**4.85**	**5.34**
A. lixula		42	3.608	-5.395	0.977	$< 10^{-3}$	**4.46**	3.608	2.627	4.955	4.46	**4.07**	**4.88**
Nanoelasticity E (GPa)													
Species	**site**	**n**	**m**	**c**	**R²**	**p-value**	**E_0(GPa)**	**mhat**	**m $CI_{95\%}$ -**	**m $CI_{95\%}$ +**	**shat**	**E_0 (GPa) $CI_{95\%}$ -**	**E_0 (GPa) $CI_{95\%}$ +**
P. lividus	Control	105	6.153	-25.927	0.885	$< 10^{-3}$	**67.61**	6.153	5.034	7.520	67.61	**65.38**	**69.92**
A. lixula		70	4.894	-19.997	0.944	$< 10^{-3}$	**59.48**	4.894	3.828	6.257	59.48	**56.48**	**62.64**
P. lividus	Acidified	98	6.741	-28.258	0.974	$< 10^{-3}$	**66.15**	6.741	5.477	8.297	66.15	**64.08**	**68.28**
A. lixula		41	4.991	-20.156	0.931	$< 10^{-3}$	**56.73**	4.991	3.621	6.881	56.73	**53.09**	**60.62**

S10. Relative quantity of gene expression of specimens from acidified site, after normalizations with *z12.1* reference gene of *P. lividus* and *A. lixula*, respectively and comparisons (n crossings) to calibrators specimens assumed as 1.

Reference gene	Target genes	*P. lividus* Relative quantity (Arbitrary units)	*n crossings*	p_{ANOVA}
z12.1	*p19*	1.765 ± 0.938	71	0.878
	msp130	1.269 ± 0.312	99	0.998
	sm50	0.619 ± 0.133	104	0.035
	can	0.960 ± 0.416	90	0.776

Reference gene	Target genes	*A. lixula* Relative quantity (Arbitrary units)	*n crossings*	p_{ANOVA}
z12.1	*p19*	0.466 ± 0.177	75	$<10^{-3}$
	msp130	0.367 ± 0.147	82	0.001
	sm50	0.317 ± 0.120	51	$<10^{-3}$
	can	0.536 ± 0.172	54	0.005

S11. ANOVA model III on gene expression of *p19*, *msp130*, *sm50* and *can* of *P. lividus* and *A. lixula* (Individual (ind) : fixed factor, crossed individual (corss_ind): fixed factor nested in individual, gene: fixed factor nested in crossed individual, qPCRassays : random factor nested in gene)

Arbacia lixula						
Factor	**Sum of squares**	**Numerator df**	**Denominator df**	**Mean square**	**F-ratio**	**p_{ANOVA}**
Gene	**11.09113**	**4**	**20**	**2.77278**	**13.898**	**$<10^{-3}$**
Individual(Gene)	4.00697	20	87	0.20035		
Controlcrossedind(Individual(gene))	8.47246	87		0.09738		
Total Error	30.567	202		0.15132		
Paracentrotus lividus						
Gene	47.80546	4	20	11.95137	21.89853	**$<10^{-3}$**
Individual(Gene)	54.15772	20	132	2.70789	4.96167	
Controlcrossedind(Individual(gene))	80.720	132		0.61151	1.12048	
Total Error	159.362	292		0.54576		

Alvares, K., Dixit, S.N., Lux, E., Veis, A., 2009. Echinoderm phosphorylated matrix proteins UTMP16 and UTMP19 have different functions in sea urchin tooth mineralization. J. Biol. Chem. 284, 26149–26160. https://doi.org/10.1074/jbc.M109.024018

Ameye, L., Hermann, R., Killian, C., Wilt, F., Dubois, P., 1999. Ultrastructural localization of proteins involved in sea urchin biomineralization. J. Histochem. Cytochem. 47, 1189–200.

Anstrom, J.A., Chin, J.E., Leaf, D.S., Parks, A.L., Raff, R.A., 1987. Localization and expression of msp130, a primary mesenchyme lineage-specific cell surface protein of the sea urchin embryo. Development 101, 255–265.

Costa, C., Karakostis, K., Zito, F., Matranga, V., 2012. Phylogenetic analysis and expression patterns of p16 and p19 in Paracentrotus lividus embryos. Dev. Genes Evol. 222, 245–251. https://doi.org/10.1007/s00427-012-0405-9

Costa, C., Pinsino, A., Bonaventura, R., Russo, R., Zito, F., Matranga, V., 2019. A pilot study for an innovative approach highlighting Actin and COI mRNAs as potential biomarkers of quality of the edible crustacean Nephrops norvegicus (Linnaeus , 1758). Food Control 97, 58–66. https://doi.org/10.1016/j.foodcont.2018.10.003

Farach-Carson, M.C., Carson, D.D., Collier, J.L., Lennarz, W.J., Park, H.R., Wright, G.C., 1989. A calcium-binding, asparagine-linked oligosaccharide is involved in skeleton formation in the sea urchin embryo. J. Cell Biol. 109, 1289–1299. https://doi.org/10.1083/jcb.109.3.1289

Illies, M.R., Peeler, M.T., Dechtiaruk, A.M., Ettensohn, C. a, 2002. Identification and developmental expression of new biomineralization proteins in the sea urchin Strongylocentrotus purpuratus. Dev. Genes Evol. 212, 419–31. https://doi.org/10.1007/s00427-002-0261-0

Jain, G., Pendola, M., Huang, Y.C., Gebauer, D., Evans, J.S., 2017. A Model Sea Urchin Spicule Matrix Protein, rSpSM50, Is a Hydrogelator That Modifies and Organizes the Mineralization Process. Biochemistry 56, 2663–2675. https://doi.org/10.1021/acs.biochem.7b00083

Karakostis, K., Costa, C., Zito, F., Brümmer, F., Matranga, V., 2016a. Characterization of an Alpha Type Carbonic Anhydrase from Paracentrotus lividus Sea Urchin Embryos. Mar. Biotechnol. 18, 384–395. https://doi.org/10.1007/s10126-016-9701-0

Leaf, D.S., Anstrom, J.A., Chin, J.E., Harkey, M.A., Showman, R.M., Raff, R.A., 1987. Antibodies to a fusion protein identify a cDNA clone encoding msp130, a primary mesenchyme-specific cell surface protein of the sea urchin embryo. Dev. Biol. 121, 29–40. https://doi.org/10.1016/0012-1606(87)90135-7

Mann, K., Poustka, A.J., Mann, M., 2008. The sea urchin (Strongylocentrotus purpuratus) test and spine proteomes. Proteome Sci. 6, 1–10. https://doi.org/10.1186/1477-5956-6-22

Sucov, H.M., Benson, S., Robinson, J.J., Britten, R.J., Wilt, F., Davidson, E.H., 1987. A lineage-specific gene encoding a major matrix protein of the sea urchin embryo spicule. II. Structure of the gene and derived sequence of the protein. Dev. Biol. 120, 507–519. https://doi.org/10.1016/0012-1606(87)90254-5